ISSN 0140 3818
SSSU 67

UNIVERSITY OF SOUTHAMPTON

DEPARTMENT OF SHIP SCIENCE

FACULTY OF ENGINEERING AND APPLIED SCIENCE

FATIGUE CHARACTERISTICS OF FRP SANDWICH BEAMS FOR MARINE APPLICATIONS

S.D. Clark, R.A. Shenoi & H.G. Allen

Ship Science Report No. 67

May 1993

ISSN 0140 3818
SSSU 67

UNIVERSITY OF SOUTHAMPTON

DEPARTMENT OF SHIP SCIENCE

FACULTY OF ENGINEERING AND APPLIED SCIENCE

FATIGUE CHARACTERISTICS OF FRP SANDWICH BEAMS FOR MARINE APPLICATIONS

S.D. Clark, R.A. Shenoi & H.G. Allen

Ship Science Report No. 67

May 1993

FATIGUE CHARACTERISTICS OF FRP SANDWICH BEAMS FOR MARINE APPLICATIONS

First Six Monthly Report

DTI / SERC Link Structural Composites Programme

Royal National Lifeboat Institution

by

S.D Clark, R.A Shenoi
(Dept of Ship Science, University of Southampton)

H.G Allen
(Dept of Civil Engineering, University of Southampton)

MAY 1993

CONTENTS

1.0 Introduction

High speed, high performance craft are becoming increasingly viable in the marine context. They are being required for diverse operations such as defense, sport, leisure, passenger ferrying and lifesaving. The operating requirements for these craft are extremely demanding thus placing tight constraints on design. The principle thrust of such constraints leads towards weight criticality of the hull structural envelope. This is forcing designers towards weight efficient material and structural topologies. The favoured material in most cases is FRP composites. Furthermore, it has been proven that for small craft where high local stiffness is important, a sandwich configuration is most apt.

Theoretical approaches to characterise sandwich structure behaviour have been available for a number of years. However, it is only recently that these have begun to find application for marine panels. The main areas of such studies have been towards understanding the static behaviour of sandwich beams and panels. Furthermore, the bulk of FRP applications in marine structures up to now were constrained by stiffness limits imposed on design. Consequently the structures, even at high loads, tended to achieve relatively low strain levels where fatigue does not pose a problem.

This aspect of design has changed and the design scenarios nowadays require structures/materials to be pushed towards the strain and strength limits. This has led to the need to seek understanding of the long term behaviour of sandwich panels under the kind of load regimes prevalent in small craft via high lateral pressures. Ultimately such studies ought to examine the behaviour of plate panels. However the first step in this direction is to understand behaviour of beams.

The purpose of this report is to review available literature in the FRP sandwich area, outline behaviour of some FRP sandwich configurations under static loads and introduce some results from fatigue testing of these panels. The tests have been conducted using a previously designed apparatus whose principal features are outlined in the Appendix.

2.0 Literature Review

2.1 Background to Sandwich Beams

2.1.1 Design Aspects - Marine Applications

The use of FRP in marine applications is becoming widespread because it is a cost-efficient, lightweight rigid structure which is corrosion resistant and needs only minimal maintenance. The GRP sandwich technique was first developed in the late 1960's with the aim of using this technique for a new series of minesweepers for the Royal Swedish Navy (1). The very first ship hull constructed in GRP sandwich was a mine sweeper, the 'Viksten' in 1974. Since then the GRP sandwich technique has successfully been used in numerous other vessels including coastguard ships, police launches and trawlers.

Sandwich structures are used for two primary reasons:
-in minesweepers because of their non-magnetic properties, rough handling ability and withstanding underwater explosions (2,3,4);
-in high speed craft due to their excellent stiffness/weight ratio and impact performance if correctly designed.

New materials and construction techniques have been developed and these have resulted in a constant improvement in sandwich properties (1,5). However, Olsson and Lonno (5) suggest that for high speed marine vessels conventional test methods do not account for load cases incorporating slamming, fatigue or impact and therefore are insufficient to determine relevant material properties. The potential for sandwich structures cannot therefore be fully utilised and the risk of faulty design is apparent. There is consequently a requirement for further research and development especially for long term loading effects.

2.1.2 Composition and Philosophy

Sandwich beams consist of a relatively low density core sandwiched between two stiff skin materials. The combination produces a relatively strong lightweight

beam, which can be used as an efficient structural component for supporting axial and/or flexural loads. The bending stiffness of this arrangement is much greater than that of a single solid plate of the same total weight made of the same material as the faces. Under flexural loads, the sandwich beam behaves in a similar fashion to an I-beam where the flange (face) material supports the bending moment in the section. The web (core) material supports the shear force at the section. An efficient sandwich structure will have thin faces and a core which is not too flexible in shear, but the choice of core materials is often influenced by practical considerations.

When in bending, the core material must be stiff enough to ensure the faces remain a fixed distance apart, and stiff enough in shear to prevent the faces from sliding over each other. The degree of stiffness in the core directly influences the amount of shear deformation: low modulus core materials show significant shear deflection; high modulus cores are stiff enough for shear effects to be small.

2.1.3 Materials in Sandwich Structural Design

There is much literature on FRP materials used in marine applications (6,7,8) in particular the calculation of mechanical properties (6,7,9). An insight into the principles which have to be understood for effective design and manufacture of structural engineering composite components is also widely reported (7,9,10,11). For sandwich structures the mechanical properties are only calculable by knowing the individual properties of the two skins and the core.

A) Skin Material

The skin (laminate) material can be made up of a number of plies of varying fibres set in (polyester or epoxy) resin matrix. References (7,9,12,13) contain properties of many types of fibre and matrix materials useful in design calculations. In general, glass fibres are the cheapest and have good all round properties. Kevlar is exceptional in impact and shows very high strength to

weight ratios but is poor in compression and shows large amounts of creep. Carbon fibres have a high stiffness and therefore are excellent in fatigue and creep. However it can be quite a brittle material. There are many types of resin but epoxy resins show very good all round performance. Unidirectional laminates display virtually perfectly elastic behaviour up until failure under uni-axial tension, but some angle ply laminates exhibit non-linear behaviour (14).

Analysis using the 'rule of mixtures' (6,10) and simple design equations (12) can give approximations to finding the longitudinal, transverse and shear moduli, and the corresponding Poisson's ratios for composite layers. By using these mechanical properties for each layer, references (7,9,15) contain information for the derivation of the overall constitutive matrix equation of a laminate. This can then be used to calculate direct and shear stresses and strains subject to external forces and moments. However lamination theory does not provide for interlaminar effects.

B) Core Material

There are many core materials used in sandwich construction. They are typically rigid and of low density. Cores can be in the form of a honeycomb structure and can be made from woven cloths of glass, carbon and nylon fibres, kraft or aramid paper, or from metals such as aluminium. Honeycomb cores are expensive but they have the highest compression, shear and stiffness properties of all core materials of an equivalent density. The most commonly used honeycomb core material with perhaps the best all-round properties is aramid fibre paper or Nomex. Balsa is the lightest commercially available wood and one of the cheapest core materials. The usual form is the end-grain type, which has good all-round properties except for its high absorbancy. The passage of water vapour through the skin over time may result in damp or saturated cores thus its use can only safely be limited to interiors. Foam cores are the most commonly used core materials for sandwich structures in the marine environment and can be either of open or closed cell form. The closed cell form is usually favoured due to its watertight integrity. Among the different foams used are polystyrenes, polyurethanes, flexibilised polyurethanes, acrylics, poly-vinyl-chlorides (PVC's)

and syntactic resins. Closed celled PVC foams are often used and they can be of the linear elastic type or cross linked with polyurethane to give greater stiffness. Cross linked PVC's have good compressive and shear properties and are characteristically stiff but brittle. The linear PVC foam is considerably weaker in compression, slightly weaker in shear, but is not brittle and has good impact properties as it will yield and then recover. Allen and Raybould (16) give a basic overview of various core materials and the selection criteria for them. Caprino and Teti (17) give some basic data for polyurethane and PVC foams and shows there is a linear relation between compression strength and compression modulus and shear strength and shear modulus with respect to core density. Further information on Airex core materials and their dependence on strain rate are given in reference (18).

2.2 Sandwich Structure Analysis - Bending of Beams

2.2.1 Analytical Closed Form Methods

For static analysis of sandwich beams, classical beam theory is a well known method for calculating section properties such as flexural stiffness and is covered by numerous sources (6,7,13,16,17,19). Allen (19,20) suggests that sandwich beams can be classified into three regimes; composite beam behaviour where core shear strains are small; thin-face sandwich behaviour where core shear strains lead to significant additional deflections; and thick-face sandwich behaviour where the load is split into two parts, one resisted by a beam analogous to a thin-face sandwich beam, and the other by a local bending action of the faces themselves. However the most common case is thin-face sandwich behaviour and a realistic assumption is that the core makes no contribution to the bending stiffness of the sandwich, so that the shear stress is approximately uniform throughout the depth of the core. Bending and shear deflections and stresses are therefore easily calculated for different boundary conditions and loading cases. For simply supported beams the shear deflection occurs quite independently of the bending deflection and has no major effect on the stresses

in the faces (20). In practice for marine applications, the faces are not always of equal thickness because FRP is weaker in compression than in tension. The bottom exterior face is therefore thicker, partly as it is in compression and partly as it is more likely to be over-engineered as it the first line of defence against water penetration. Classical beam theory can still accommodate this if the position of the actual neutral axis is found.

Theulen and Peijs (21) give an optimisation of bending stiffness and strength as design parameters. This can be extended to plate theory in three dimensions for various loading conditions assuming isotropic or orthotropic material properties (19). Design data for marine sandwich composites can be found in references (7,13,22).

2.2.2 Numerical Solution Techniques

The most common form of analysis is finite element analysis and there are numerous references (23,24,25,26,27) covering the basic principles. The finite element method (FEM) uses basic principles of elasticity on a mesh of identical representative elements substituted for the actual structure. The most common form of FEM is the displacement based method. The steps in the typical solution for a linear elastic structural problem (27) is as follows:

-Idealisation of the structural problem.
-Subdivision of the continuum in finite elements.
-Modelling of the displacement field for each finite element.
-Generation of the stiffness matrices and the nodal equivalent loads for each element.
-Assembling the element stiffness matrices into a global stiffness matrix, taking into account the connections between the elements.
-Specifying the displacement boundary conditions.
-Solution of all equilibrium equations to obtain all element nodal point displacements.
-Evaluation of the element stresses by equations relating displacements to strains and stresses.

2.2.3 Failure Modes in Flexure

A) Skin Failure

In bending, with increasing load the failure mechanisms of skin materials on the tension face (6,9,12) include: fibre matrix decohesion (interfacial debonding), fibres breaking at weak points (glassy fibres have a variability of strength due to there being a distribution of flaws along their length), microcracking of the matrix between debonded fibres and at fibre ends and eventually fibre pull out and consequent rupture. Crack extension is generally preceded by delamination between plies of different orientations and splitting within them. This can involve crack growth in the matrix (transverse ply cracking) and at the fibre-matrix interface. All of these mechanisms of failure can combine in a variety of ways to give a number of options of macroscopic fracture behaviour and complex paths of crack propagation.

In bending, on the compression face the phenomenon of crimping or wrinkling (19) can happen (the material tries to fold itself on itself) and this is caused by the skins being too thin and having too low a shear modulus.

B) Core Material

The mechanisms of failure are largely dependent on the core material and its properties. General failure of PVC foams by core shear, may be shear fracture resulting in catastrophic failure in the case of cross linked foams or simply excessive deflections by plastic yielding of the material in the case of linear elastic foams. Balsa cores however fail by grains tearing and pulling apart. For all materials there is a strong dependence of shear deflections on core density.

Localised failure may assume two different forms according to the kind of core material used (17). In the case of foams, the contact between facing and core is continuous and localised failure requires failure of the bonding at the interface and/or the failure of the core itself. With honeycomb cores, the bonding of core to skin is only on the cell walls. When the facings are subjected to compression,

they may therefore undergo buckling in the free spaces within single cells generating a dimpling phenomenon. This can easily be rectified by using thicker facings or decreasing the core cell size.

2.3 Fatigue of Sandwich Structures

2.3.1 Fatigue of Skins

A) Fatigue Damage Mechanisms

There are three basic failure mechanisms in composite materials associated with fatigue; i.e matrix cracking, interfacial debonding and fibre breakage (29).

(i) Unidirectional fibres

Damage mechanisms of unidirectional fibre composites in tensile fatigue have been extensively investigated (30). For unidirectional composites the fibres carry virtually all the load but experimental evidence suggests fatigue performance is determined principally by the strain in the matrix (31,32). All non-metallic fibres have a statistical distribution of strength, determined by flaws; thus a few of the weakest fibres will fail during fatigue loading. Locally high stresses in the matrix and at the fibre/matrix interface lead to the development of fatigue damage. Damage may also develop at local micro defects, such as misaligned fibres, resin rich areas or voids. These can lead to resin cracks developing between fibres, isolating them from adjacent material, rendering them as ineffective load carriers causing fibres to become locally overloaded, resulting in further fibre static failure. Close to failure, the matrix may show extensive longitudinal splitting parallel to fibres caused by resin and interfacial damage, leading to the brush like failure characteristic of most unidirectional materials (31).

Unidirectional composites characteristically show excellent fatigue resistance (32). However since fatigue performance is linked mainly to the strain in the matrix, the use of stiffer fibres will only show a slight increase in fatigue performance compared to using a modified fatigue resistant resin. The slope of the S-N curve is related directly to the strain in the matrix (31). Glass fibres with failure strains of 2.5-3.5% lead to greater matrix strains when compared to carbon fibres with failure strains of 0.6-1.8%: therefore the slope of the S-N curve for the former case is greater. With aramid fibres the fatigue damage mechanism is more complicated since the aramid fibres are themselves fatigue sensitive and can defibrillate during fatigue loading. This causes the S-N curve to adopt a flat shape which becomes much steeper at an intermediate number of cycles (see Figure 2.1). Talreja (30) suggests that the shape of the strain life diagram depends on the relation between the static failure strain of the composite and the fatigue limit of the matrix. According to this view, if the matrix fatigue limit is greater than the static failure strain of the composite, broken fibres occur at random during cycling and the life dependence is statically determined. If on the other hand, the matrix fatigue limit is less than the static failure strain of the composite, progressive fibre fracture can occur (perhaps in association with matrix cracking and fibre matrix debonding) and a sloping curve results which is stress and cycle dependant.

(ii) Laminates

Composite materials are usually formed with a combination of several laminae in various directions, with a stacking sequence based on design load requirements. Matrix cracking in off-axis plies is usually the first significant damage and grows during fatigue cycling across the laminate (32,33). Transverse cracks couple together by interface debonding enhanced by tensile stresses; this mechanism leads to transverse cracks in one lamina spreading into neighbouring laminae. Longitudinal cracking caused by stacking sequence related edge stresses may also assist in crack coupling. An intense damage region then forms where delaminations grow driven by interlaminar stresses and some fibre fracture takes place in the 0° plies eventually causing specimen rupture. However the ultimate tensile fatigue failure of composites is still usually determined by the

unidirectional layers. Thus the tensile S-N curves for multi-directional laminated composites are still relatively shallow, although steeper than for fully uni-directional composites (30).

B) Frequency Effects

Under cyclic load, hysteresis heating effects increase noticeably for increasing frequency. This heating effect is particularly apparent in resin rich (low volume fraction) laminates (31). In GRP the greater the rate of testing, the greater the strength. Thus when collecting data for fatigue tests, it is desirable to carry out static tests at the same strain rate as fatigue tests. For sandwich structures, increasing the frequency results in the core getting stronger and stiffer with corresponding temperature rises in the core (2). Results show that for a frequency of 3 Hz, the temperature rise is about 10°C at a shear stress level of about 45% of the ultimate shear stress, while at 5 Hz the corresponding temperature rise is about 30°C.

C) Edge effects

Edge induced stresses are especially a problem in fatigue and testing policy is usually aimed at minimising edge effects and the damage that inevitably results. Both shear and normal stresses can develop at coupon edges; these arise from a mismatch of properties between the layers (31). The magnitude of the stresses change both with temperature (as layers have different expansion coefficients) and also with moisture content (as layers expand to different extents on absorbing external moisture). Thus layer stacking sequence is a critical variable. In general, laminates with evenly distributed layers lead to the lowest edge effects for both tensile and compressive externally applied loads.

2.3.2 Fatigue Damage Modelling

A) Statistical Representation of Data

The traditional curve of applied mean stress level against number of cycles to failure (S-N curve) forms the oldest and most voluminous form of fatigue data presentation. However its usefulness is limited because a separate curve for every material, condition, shape, size must be obtained (34). Attempts to plot S-logN often showed that the function was not only nonlinear but nonexponential and that the hoped for constant exponent in the damage law equation was not really a material constant after all. The number of cycles to failure depends on the stress range and mean stress. Gerber proposed a parabolic relation whereby the endurance limit and/or curves of constant life can be plotted (see Figure 2.2a). Goodmans diagrams, with linear relationships, are a useful means of presenting fatigue data, but in general form (see Figure 2.2b) the upper and lower range limits are for infinite life. The need to include the stress ratio R as well as mean stress resulted in the evolution of the Constant Life Diagram (see Figure 2.2c). These plots indicate the behaviour in terms of constant life lines for all conditions that are possible to apply. The information is contained entirely within the Goodman line triangles; regions outside the static boundaries represent stresses greater than the ultimate strengths. The diagrams may be regarded as a collection of S-N curves, each at the appropriate mean stress and stress ratio.

B) Modelling

The most widespread technique for the life prediction of metallic components is linear elastic fracture mechanics, which is based on the growth of single flaws to failure. In composite materials fatigue is associated with the growth of multiple micro-cracks in the matrix and therefore the applicability of such a technique is severely limited (31,35). Current techniques that have been developed are based on the phenomenological approach which is concerned with lifetime predictions without enquiring into the microstructural nature of fatigue

failure within the composite (35). This approach falls into two categories, namely empirical models and wear-out models.

Empirical models are often statistically based, thus requiring large amounts of data such as static strength, fatigue life and residual stress distributions in order to predict residual strength at any number of cycles. Wear out models are all physically based, relating to the reduction of some physical property such as stiffness or strength, and the ability to predict its decay during fatigue loading. However a problem arises since the chosen wear out parameter is inevitably dependent on stress. Therefore testing at various stress levels must be undertaken to describe its behaviour.

Many phenomenological approaches have been proposed, each with its own failure criterion depending on the degradation variable used. One approach is to measure residual strength with load cycling. Then an S-N curve can be drawn through the focus of data points where the residual strength equals the applied stress. If the application is critical, a Weibull distribution could be used to describe the variations in strengths and probability curves can be drawn through the vast collection of data. Many approaches assume that failure will occur when some critical level of damage in the composite is exceeded (6). Damage grows with cycling and its growth depends on the cyclic stress range, the load ratio and the current value of damage provided other variables such as temperature and frequency do not change. It follows that the fatigue lifetime is simply the number of load cycles it takes to raise an initial damage state (usually equal to zero) to the final or critical level of damage. The problem is the damage function is not known but this can be associated with the reduction of some property such as stiffness which can be gathered experimentally. Testing procedures and standards for static and fatigue testing are outlined in reference (28).

Broutman and Sahu (36) proposed a new cumulative linear damage theory based on the reduction of the elastic modulus. Hahn and Kim (37) introduced a non-linear residual strength model using secant modulus degradation. Charewicz and Daniel (38) proposed a damage model based on the assumption that the residual strength

degradation rate is a function of the life fraction n/N, but not residual strength. Also Hwang and Han (39) introduced a model based on the fatigue modulus concept where during fatigue cycling, the stress-strain curve changes causing a reduction of fatigue modulus.

2.3.3 Fatigue at the Interface

Composite materials owe their very existence to adhesion between resin matrix and reinforcement and additionally with core materials. This requires a tough adhesive which is compatible with the skin and core material. Consideration needs to be given to the stress regime, joint geometry and fabrication methods proposed. Additionally the mechanical, thermal, creep and durability properties of the adhesive must be considered before selection.

In general, toughened adhesives in the top of the acrylic stiffness range and the spectrum of cold/warm cure two part epoxies are all true structural adhesives for FRP applications. The fatigue characteristics of the interface of sandwich structures is generally excellent if loading is moderate. Peak stress levels should at all times be designed to cycle within the elastic range of the adhesive. It follows that cyclic loads should be maintained significantly lower than the limit loads indicated by static results. However debonding of the skin from the core can take place especially during high rate dynamic loading like slamming, impact, and explosive shocks as often encountered in the marine environment (5). Several debonding failures have been encountered by coastal rescue vessels in Norway (40) where there was an underestimation of loads experienced in the design and approval of the vessel. Some core adhesives are considerably stiffer than the core materials they are expected to join. Thus when loaded, they develop appreciably higher stresses than the surrounding foam core. With repetitive slamming loads the low ductility adhesive cracks at an early stage and the foam core takes on a more brittle, less damage tolerant behaviour. The crack in the adhesive can initiate cracking in the core. Thus it is important to match the properties of adhesive and core as closely as possible and to ensure the combination is damage tolerant.

2.3.4 Core Fatigue

In sandwich structures under a cyclic load, failure of the core is usually associated with core shear. Methods of testing are given in ASTM Standards for Composite Materials (41). Loading is in shear parallel to the plane of the facings. From a complete load deformation curve it is possible to compute shear stress of the sandwich or core at any load and to compute an effective shear modulus. However there is a dependence of the results on the test method used, and no core shear values should be incorporated into design calculations without a full knowledge of the testing procedure and laboratory conditions (28).

Recent developments in Sweden (5) have concluded that at high strain rates the core material becomes more brittle and hence the ultimate stress and modulus increase while the strain at ultimate stress decreases with increasing strain rate. During cyclic loading this may mean the material is less damage tolerant and more susceptible to crack propagation (40). Buene and Hayman (42) give two core failure modes which are common in fatigue, as indicated by Figure 2.3. The mode 1 failure was characterised by a single shear crack indicative of fracture initiation by shear cracking and is more typical of brittle cross linked foams. In mode 2, the final shear failure is associated with cracks in a progressively damaged horizontal region in the core and indicates weakening of the core by progressive damage and subsequent yielding. This is more typical of linear foams.

2.4 Creep Behaviour of Sandwich Structures

2.4.1 General Behaviour

Under long term loading conditions such as the continuous application of a cyclic load, the response of a sandwich beam is time dependent (43). The materials response may no longer be elastic and the deformation may no longer provide a linear correspondence between stress and strain. In fatigue or indeed under a constant load, a gradual increase in deflection (which may be permanent) is observed with time. It is this resulting deformation that is influenced by so-called viscous effects. This visco-elastic phenomenon is called creep.

A typical creep curve (see Figure 2.4a) has three distinct stages (44). The first is that of primary creep which is largely visco-elastic and therefore partly recoverable. It is characterised by a uniform deceleration of the creep rate which never reaches a constant value. Secondary or steady state creep (at a constant rate) is irrecoverable by nature and is characterised by a straight line when plotting strain against time. Tertiary creep is that of rapidly accelerating creep before creep rupture. Different materials differ in the arrangement of the three regimes. Creep curves are strongly influenced by stress and temperature. Figures 2.4 b,c&d show that below a certain threshold no creep occurs.

2.4.2 Creep Mechanisms

There are two main creep mechanisms (27). The first is diffusional creep and the second is dislocation creep. Diffusional creep occurs by the bulk movement of atoms from one atomic site under compression to another in tension. Diffusional creep at low stresses exhibits a more or less linear viscous dependence on stress. In engineering structures the most important mechanism is dislocation creep. Defects known as dislocations in the crystal lattice structure overcome the natural stiffness of the lattice and obstacles (impurities), and move through the lattice. At low stresses the dislocation stops or slows down and has a high non-linear dependence on stress. In foam material, this may be said to correspond to a movement of dislocations along cell-wall boundaries.

2.4.3 Creep Modelling

There have been many attempts to model creep behaviour but there is little reference to creep in sandwich structures. Many standard text books cover the basic principles of elastic and plastic flow in metals under long term loading (44,45,46,47,48). These references show that many approaches assuming steady state creep and a uniaxial state of stress, start with the Bailey/Norton law and use either the strain-hardening or time-hardening formulation to model steady state creep under uniform, variable or cyclic load. Multi-axial stress states are

an extension to uni-axial models and application necessitates tensor analysis (46,55). Transient creep methods which include the effect of stress redistribution in the material assume more importance for variable loading but are invariably complicated and normally result in indeterminate solutions which have to be solved numerically (46).

A) Application to Laminates

Composite materials are visco-elastic in nature and basic models consist of various combinations of springs and dashpots connected together. Gittus (45) and Rabotrov (48) include the basic visco-elastic Maxwell and Kelvin models. Most linear visco-elastic analysis is based on finding a suitable creep compliance and via the correspondence principle, substituting the elastic modulus in static laminate analysis, with the inverse of the creep compliance (49). The creep compliance can be of an exponential (43), or power law (50) form under constant load, and a harmonic function under cyclic load (49). It is a function of material dependent constants and time under load. These constants can, in general, only be determined by comparing similar laminates with known constants, or testing the laminate itself in creep (for testing methods see reference (52)). Real GRP laminate materials display an initial elastic response where the rate of creep decelerates until the rate of creep can be approximated as being steady at some time t_0. The problem is that this time t_0 (which is dependent on laminate relaxation time) needs to be determined, and therefore knowledge of the material relaxation time is essential (51).

B) Application to Sandwich Structures

In sandwich structures because of the relatively low density core, the beam/panel can display a significant visco-elastic response. In fact, the key element in the creep of sandwich structures is the response of the core. Unfortunately very little information exists on creep of core materials (5,43,53,54). A rough comparison of the creep of various core materials is given in Figure 2.5. Chevalier (54) shows that the rate of creep is in proportion to the core density and material structure. Lower densities display more creep and linear PVC foams

creep substantially more than cross-linked types. The modelling of creep in sandwich structures is similar to that for laminates. One approach (43) was to model the beam by a stepwise change in the stress function where the material 'remembers' its prior deformed length and deforms increasingly from that point in time. A Kelvin model was chosen for simplicity and a suitable creep compliance determined from experimentation.

3.0 Characterisation of Sandwich Beams under Static Load

3.1 Background

The sandwich beams being studied in this testing programme are to be applied in hull forms of high performance lifeboats. The operational conditions that predominate, are those of large scale repetitive slamming pressures where average encounter frequencies of about 0.3 Hz on average are common. Over an expected life service of about 20 years the lifeboat hullform will have encountered about five million impacts.

The structural panels in the hulls, are idealised as beams which are simply supported at the edges. The slamming pressures encountered are idealised as uniformly distributed pressure loads over the total span of the beam. The load is applied with the thick skin in compression and the thin skin in tension.

The chosen span is 1300mm, and the beam width is 200mm. A core thickness of 50mm gives a total beam depth of 58.5mm. Independent static testing on the facings was carried out in an Instron machine (57) and the resultant properties are given in Table 3.1. The core material properties obtained from manufacturers data are given in Table 3.2.

The beams have identical faces made from hybrid glass and kevlar fibres set in epoxy resin. The core materials tested in the main group, are linear PVC foam (Airex R63.80) and cross linked PVC foam (Airex R90.200). Additional static tests on balsa and Divinycel H200 were also made for experimental comparison purposes. The resulting load-deflection curves are plotted in Figure 3.1.

3.2 Analytical Treatment of Beam Behaviour

3.2.1 Section Properties and Stresses

a) Flexural Rigidity

It is assumed that the beam is narrow and that it bends anticlastically. The load must also be applied be symmetrically. The beam may be treated as a homogeneous isotropic element. From classical beam theory for a simply supported beam under uniform load (see Figure 3.2a), the maximum bending moment occurring at the beam centre is :

$$M_{(max)} = \frac{\omega l^2}{8} \qquad (3.1)$$

The maximum shear force occurs at the supports and is of magnitude :

$$Q_{(max)} = \frac{\omega l}{2} \qquad (3.2)$$

The flexural rigidity, D of a beam is the sum of the product of the Young's modulus and the second moment of area about the whole beams neutral axis for each component. For the beam under consideration (see Figures 3.2b & 3.3), the skins are of unequal thickness, thicknesses t_1 and t_2 with corresponding Young's moduli E_1 and E_2 respectively. The core thickness, c has Young's modulus E_c. Therefore :

$$D = E_1 bt_1d_1^2 + E_2 bt_2d_2^2 \qquad (3.3)$$

where :

b - beam width
d - distance between neutral axis of the facings
d_1 - distance from beam neutral axis to neutral axis of top facing
d_2 - distance from beam neutral axis to neutral axis of bottom facing

assuming :

a) the faces are thin so that the second moment of area about their own neutral axis is negligible.

b) the core makes a negligible contribution to the flexural stiffness of the sandwich hence the shear stress is approximately uniform throughout the core.

Both of these assumptions are valid in the case of the beams tested.

In a more convenient form from Reference (58) :

$$D = bd^2E_1t_1\left[\frac{(E_2t_2 / E_1t_1)}{1 + (E_2t_2 / E_1t_1)}\right] \qquad (3.4)$$

b) Stresses

The bending stresses in the faces may be determined by ordinary bending theory. As sections remain plane and perpendicular to the longitudinal axis, the strains at any distance z below the neutral axis are Mz/D.

The stress on the faces (6) is :

$$\sigma_f = \pm \frac{Mz}{D} \cdot E_f \qquad (3.5)$$

Now $\sigma_{(max)}$ occurs at z = ± h/2 and from Equation 3.1 :

$$(\sigma_f)_{max} = \frac{\omega l^2}{16} \cdot \frac{hE_f}{D} \qquad (3.6)$$

For a homogeneous beam the shear stress, τ at depth z below the centroid of the cross section (19), is :

$$\tau = \frac{Q}{Db} \sum (SE) \qquad (3.7)$$

S - first moment of area of that part of the section for which $z > z_1$
E - Young's modulus
b - width at level z
Q - shear force

Using the same assumptions as for calculating D (i.e assuming the shear stress distribution in Figure 3.4c), the shear stress in the core reduces to :

$$\tau = \frac{Q}{bd} \qquad (3.8)$$

This is associated with shear strain :

$$\gamma = \frac{Q}{Gbd} \qquad (3.9)$$

where G is the shear modulus of the core and Q is the shear force. The stress distribution in a sandwich beam is illustrated in Figure 3.4. The shear force, Q at a distance x from one end of the beam is :

$$Q = \omega x - \frac{\omega l}{2} \qquad (3.10)$$

3.2.2 Deflections

The bending deflection, Δ_1 at mid-span of a uniformly simply supported beam is given as :

$$\Delta_1 = \frac{5\omega l^4}{384D} \qquad (3.11)$$

where D is defined in Equation 3.4.

There is also an additional shear defection, Δ_2 caused by core shear. This occurs quite independently from the bending deflection and has no major effect on the stresses in the faces (20).

From Figure 3.5 showing a section of sandwich in shear (19), and using Equation 3.9 :

$$\frac{d\Delta_2}{dx} = \gamma.\frac{c}{d} = \frac{Q}{Gbd}.\frac{c}{d} = \frac{Q}{AG} \qquad (3.12)$$

where :

$$A = \frac{bd^2}{c}$$

From substituting Equation 3.10 into Equation 3.12 and integrating, it is seen that :

$$\Delta_2 = \frac{\omega x^2}{2AG} - \frac{\omega l x}{2AG} \qquad (3.13)$$

At midspan :

$$x = \frac{l}{2} \qquad \therefore \quad \Delta_2 = \frac{\omega l}{8AG} \qquad (3.14)$$

The total deflection, is the sum of the bending and shear components :

$$\Delta = \Delta_1 + \Delta_2$$

$$\Delta = \frac{5\omega l^4}{384D} + \frac{\omega l^2}{8AG} \qquad (3.15)$$

From Figure 3.6, a graph is given showing the influence of the bending and shear components on overall deflection. It can be seen that the shear component is 29% of the overall deflection for the linear foam, 11% for the higher density cross-linked foam and 9% for Divinycel foam.

3.2.3 Modes of Failure

Failure can occur at the skins, the core or at the skin/core interface.

If proper sandwich beam optimisation is used (ie. beam components are of sufficient dimensions) and the beams are properly fabricated (ie. assuming the adhesive joints are tougher than the core), the three possible failure modes that could occur are :

: skin failure through compression wrinkling
: skin tensile failure
: core shear failure

The theoretical limiting load equations for each failure criterion are given by Shenoi *et. al.* (58). Because of the very high value of uniform load required to initiate wrinkling on the compression (thick) face for both types of Airex core, the wrinkling failure mode was discounted.

The limited loads for the skin, ω_s, which is assumed to be the thin skin in tension is given as :

$$\omega_s = \sigma_s \cdot \frac{8\,D}{l^2\, y_{max}\, E_s} \qquad (3.16)$$

σ_s - tensile strength of the skin

y_{max} - maximum distance from neutral axis to tensile skin outer edge

D - flexural rigidity of the beam (defined in Equation 3.4)

E_s - Young's modulus of the skin

The limiting load for the core, ω_c is given as :

$$\omega_c = \tau_c \cdot \frac{2bd}{l} \qquad (3.17)$$

τ_c - limiting shear stress in the core

3.3 Application to Low Density Linear Airex (R63.80) Foam Core

3.3.1 Load-Deflection curve

Looking at the load-deflection cure for Airex R63.80 (Figure 3.7), it shows a failure load of about 12.1 N/mm (8.8 psi). Perfectly linear behaviour was displayed up until about 6.9 N/mm (5.0 psi). From then on, the deflection rate accelerated for a constant increase in applied uniform load until large magnitude deflections occurred for virtually no increase in load.

Theoretical load deflection curves (also shown in Figure 3.7) based on linear beam theory described in Section 3.2.2 show that for the linear part of the experimental load deflection curve, theory corresponds very closely. When the experimental curve becomes non-linear, theory becomes increasingly inaccurate

with further applied load. The load at which experimental deflection becomes flat corresponds to the shear strain at which the core material begins to exhibit 'plasticity' - see Figure 3.8.

From the load deflection plot, the shear stiffness (i.e shear force/deflection versus deflection) diagrams for the beams can be plotted. The maximum shear force is approximated by Equation 3.2. A shear stiffness-deflection plot is given in Figure 3.9. It is observed that the experimental values of shear stiffness remain approximately constant until near the failure load. The core then starts yielding, stiffness then decreases slowly at a more or less constant rate with increasing load and finally levels out just before failure.

3.3.2 Deflection Components

The bending and shear components of total deflection are also shown in Figure 3.6.

The magnitude of shear deflection for a beam of given dimensions is solely dependent on the core material, in particular its ability to withstand shear. It is assumed that the shear deflection in the facings is negligible. The core shear modulus, G is dependent on its density (G increases linearly with increasing density - see Section 2.1.3b) and to a lesser extent dependent on the core material's structure (i.e linear or cross-linked). The greater the shear modulus the smaller the shear deflection as described in Section 2.1.2 and given by Equation 3.14.

The bending deflection for a beam of constant length and cross sectional area is dependent entirely on the flexural rigidity of the beam. This is a skin related phenomenon provided no failure of the core occurs, since the core has negligible flexural rigidity. Increasing D decreases the bending deflection as given by Equation 3.11. For linear foam the bending deflection accounts for 71% of the total deflection.

For a beam of constant geometry and utilising the same facings but with different core materials, it becomes apparent from Equation 3.15 that decreasing the core's shear modulus, G, will only increase the shear component of total deflection. This relationship is shown graphically in Figure 3.6.

3.3.3 Stress Magnitudes

Analysis using linear beam theory for a simply supported beam under uniform load shows an ideal maximum value of shear stress of $\omega l/2$ occurring at the supports. It would therefore be expected that if the failure mode of the beam was core shear then failure would occur at the supports. Earlier theoretical studies (57) using finite element analysis (FEA), show that the actual maximum shear force does not necessarily occur at the support and may not reach the ideal maximum value, as shown by Figure 3.10a.

For an eight point loading system (similar to the fatigue rig), the actual maximum shear stress obtained from FEA agrees well with the straight line between the end ram and the support obtained from ideal elementary thin face theory, but is about 10% less than the ideal shear stress under uniform load of $\omega l/2$ (57). (see Figure 3.10b).

However the actual maximum shear stress predicted by FEA analysis for both the uniform load case and the eight point load case, is of the same magnitude and occurs at the same location along the beam. From experimentation the failure mode was that of core shear and occurred at a distance from the supports similar to that predicted by FEA analysis of about 45mm.

3.3.4 Failure Mode

In determining theoretical failure loads in the core, one limiting criterion could be taken as being excessive (non-linear) deflections in the beam. It is therefore necessary to define failure, as the point where marked yielding of the

core occurs (the shear stress-shear strain curve for the core becomes non-linear - see Figure 3.8). It was decided to use the yield point (or linear limit) value of shear stress to satisfy this condition. A value giving a limiting shear stress value of 0.6 N/mm^2 was chosen (which is much smaller than the value of maximum shear stress quoted in Table 3.2). On this basis, ω_c was calculated (from Equation 3.17) to be 11.0 N/mm.

This highlights the inadequacy of linear beam theory and demonstrates the importance of selecting proper values of maximum core shear stress. Dependence on manufacturers data is often not wise and therefore individual testing of basic material properties is the only recourse.

Using the skin failure criterion in Equation 3.16, ω_s was calculated to be 27 N/mm. Taking the lowest uniform load depicting the actual failure mechanism, which in this case is core shear, the maximum design pressure that the beam can accommodate is equivalent to about 11.0 N/mm (8.0 psi).

3.4 Application to High Density Cross-Linked Airex (R90.200) Foam Core

3.4.1 Load-Deflection Curve

The load-deflection characteristics of Airex R90.200 foam when incorporated in a sandwich beam are shown in Figure 3.11. The failure load was not found, because the maximum stroke of the rams on the rig would not support deflections greater than 100mm, at which stage the beam had still not failed. A comparison with theoretical plots using beam theory is given in Figure 3.11. It can be seen that once again theory corresponds very well with experimentally obtained values within the linear region. The failure mechanism in this case is known to be that of tensile skin failure and takes place at the beams centre where the bending moment is greatest. However the difference between the theoretical and experimental failure deflections is expected to be far less than for linear foams

because the failure mode has changed and is related to the facings and not yielding of the core. This is because independent load-deflection testing of the facings show more linear behaviour than for core materials.

The experimental shear stiffness diagrams were obtained from the load deflection plot (see Figure 3.12) and show a constant decrease in stiffness with increasing load up until failure.

Load-deflection curves for sandwich beams with three core materials are shown in Figure 3.1. Divinycel H200 also a cross-linked PVC foam and of the same density is included as it shows very similar behaviour to Airex R90.200. Airex R63.80 linear foam is also included to put its relative performance against higher density cross-linked foams in perspective.

3.4.2 Deflection Components

The bending and shear components of total deflection are also shown in Figure 3.11. Because the shear modulus for the higher density cross-linked core is over three times greater than that for the linear foam, the shear deflection is much reduced. The bending deflection remains the same as for linear foam because the facings have not changed. In percentage terms, the bending component of total deflection therefore plays a more dominant role (89% here as compared to 71% for linear, low density foam) and theoretically failure is more likely to be associated with tensile skin failure rather than that of core shear.

3.4.3 Failure Mode

As described earlier the failure mode is skin tensile failure. When analysing theoretical failure modes, the failure load of the skin is approximated to be the same as given for linear foam since the skins have not changed and it is assumed that the increase in overall flexural rigidity from a stiffer core is negligible. Therefore as before, ω_s= 27.0 N/mm.

It would be expected that the limiting shear stress in the core defining the yield point, will be virtually equal to the ultimate shear stress, because the foam is cross linked and of higher density, and hence likely to be more brittle in nature. In this case a limiting shear stress value of 3.0 N/mm^2 was chosen directly from Table 3.2. From Equation 3.17, ω_c was calculated to be 50 N/mm.

The lowest failure value depicts the failure mode and in this case it is skin tensile failure. Therefore ω_s = 27.0 N/mm which corresponds to a load of 19.5 psi.

However experimental results indicate that Airex R90.200 has a failure load well in excess of 33 N/mm (24 psi). This casts some doubt on the experimentally obtained tensile strength (57) of the thinner tensile skin obtained from Table 3.1.

An approximate calculation was made using the rule of mixtures to calculate a tensile laminate failure stress for the thinner tensile skin. A volume fraction of about 46% and a quadraxial E-glass, Kevlar 49 and epoxy laminate was assumed with glass and kevlar being in the ratio 4 to 1 respectively. This gives an ultimate strength of 474 N/mm^2. SP Technologies technical report (see reference 61), gives a mean strength of 321 N/mm^2 for the hull inner skin. Lloyd's Register's standard practice as stated in the report is to use 90% of the mean strength as a design ultimate value. This therefore gives a design value of 289 N/mm^2.

Considering this information, it was thought that the experimentally obtained values for the facings as reported by Shenoi and Allen (57) were to low and therefore unrepresentative. It was decided to use SP Technologies experimental result on the same skin, but taking the design value of 289 N/mm^2 as given above. This corresponds to a skin failure load of ω_s = 44 N/mm (32 psi) using Equation 3.16. The experimental characterisation for this layup in a static context is shown in Figure 3.1. It can be observed that the load-deflection curve is linear with the limiting stroke of the pneumatic ram (100mm) being reached when a pressure corresponding to 33 N/mm is reached. At this stage had not failed. The

experimental characterisation therefore needs to be redone in order to confirm the theoretically obtained failure value of 44 N/mm.

This again demonstrates the importance of determining proper values for material properties, in this case the ultimate skin tensile failure stress.

4.0 Characterisation of Sandwich Beams under Fatigue loading

4.1 Background

Fatigue tests have been carried out on beams under an approximated uniform load with their ends simply supported. The cyclic load applied was approximated as of square wave form but was limited by what the pneumatic rams could achieve. A characteristic load versus time curve is shown in Figure 4.1. The cyclic loading was from a minimum value of zero to a chosen maximum value (i.e stress ratio, R = 0). In most cases, at least six beams were tested for each load. Beams were also tested at different testing frequencies, but the highest frequency attainable was dictated by the load and unload reaction times of the rams. For each of the beams tested the load was measured at two points. One at 375mm from the beam centre and the other at 75mm. The deflection was also measured at the centre of the beam. Both maximum and minimum values were recorded for all measurements, every 50 cycles for beams with a short expected life (i.e tested at high loads) and every 100 or 200 cycles for beams with a longer expected fatigue life.

Testing to date has been three-fold, and is as follows :

a) Linear PVC foam (Airex R63.80)
   Testing frequency : 0.33 Hz
   Tested at various loads ranging from 9.0 N/mm (6.5 psi) to 3.5 N/mm (2.5 psi)
   (about 45 beams have been tested)

b) Linear PVC foam (Airex R63.80)
   Variable frequency testing : 0.50, 0.91 Hz
   Loads [N/mm (psi)] : 7.6 (5.5), 6.2 (4.5), 4.8 (3.5)
   (36 beams tested)

c) Cross-linked PVC foam (Airex R90.200)
Testing frequency : 0.5 Hz
Loads [N/mm (psi)] : 24.8 (18), 22.1 (16), 19.3 (14), 16.5 (12), 13.8 (10)
(22 beams tested to date [23/4/93])

Beam Fatigue lives for each load are tabulated in Tables 4.1 a,b,c for the linear foam cored beams and Table 4.2 for the cross-linked foam cored beams. The results are presented graphically for each beam as a load-time plot and a maximum and minimum deflection-time plot. By collecting together all the fatigue data, a S-N curve can be drawn for each test frequency.

4.2 Application to Linear Airex (R63.80) Foam

4.2.1 Deflection - No. of cycles curve

A typical maximum and minimum deflection versus number of cycles plot is given in Figure 4.2. The curve shows two distinct regions. In stage 1, the beam deflection continues to increase at a constant rate for most of its life. At stage 2, the core starts to fail, and rapidly accelerating deflections occur, until failure. Failure occurs when there is a rapid loss of stiffness and beam deflection increases sharply. This is shown in Figure 4.3 where for most of the beams life a slow constant decrease in stiffness is observed until near the end of the beams fatigue life when the beams stiffness rapidly decreases until the point of failure.

It is interesting to note that the typical maximum deflection curve is very similar to a creep curve showing all the primary, secondary and tertiary creep characteristics. Korin (51) conducted creep testing on GRP laminates, and produced a deflection-time plot (see Figure 4.4), which is very similar in nature to those obtained in this fatigue testing. However to quantify the time-dependent behaviour of these materials, it is necessary to obtain the creep compliance functions. As yet, no comprehensive creep modelling exists for sandwich beams mainly because of the vast number of possible sandwich configurations. This means that individual creep testing in most cases, is still the only means of predicting creep behaviour of such specific materials.

It is expected that some detailed theoretical modelling will be done to this end, by identifying and quantifying the creep component of fatigue, thus accounting for the various stages of the fatigue deflection curve.

4.2.2 Failure Mode

For the linear foam, it was found that the dominant failure mode was core shear. Failure occurred near the supports and was associated with deflections becoming very large resulting from a loss of shear stiffness and strength in the core. This is the same as the failure mode for static testing outlined in Section 3.3.4. This does not necessarily mean that the failure mode in fatigue can be predicted from static considerations alone. Information about the fatigue behaviour of the individual components needs to be obtained and this issue will be investigated in later research. However from the limited testing to date of two types of sandwich beam, it appears that if the theoretical static failure loads for the skin and core are not too similar in magnitude, then the smallest static failure load will indeed give the failure mode in fatigue.

The maximum 'permanent set' in a failed beam occurred at an average distance of 300mm away from the supports. A typical beam profile after failure is shown in Figure 4.5. The failure characteristic was an obvious cracking and large associated permanent deformation (see Figure 4.6a) for beams lasting in excess of 50 000 cycles (i.e testing at low loads), and only a slight rippled effect and smaller permanent deformation for beams having a smaller fatigue life (i.e testing at higher loads - see Figure 4.6b).

It was noticed that the apparent 'plastic zone' marking the core shear area shown by core cracking or a slight rippled effect, was nearer the supports (20 - 80 mm) than the point of maximum permanent set (about 300 mm). This ties in with theory by FEA as described in Section 3.3.3.

Fatigue is often modelled specifically by the reduction of some physical property, such as strength or stiffness. Figure 4.7 and 4.8 show this trend. Static tests were performed on three specimens pre-fatigued at 30% of the static shear strength for 1×10^6, 2.4×10^6 & 3.75×10^6 cycles. Other than noting a reduction in strength by about 15% of the ultimate load for the beam

tested at 3.75 x 10^5 cycles (Figure 4.7), there are two other points worth noting. Firstly appreciable residual plastic distortion takes place after fatigue loading. These are shown in Figure 4.7 by the intersection of the curves with the deflection axis. A permanent deformation of 15mm was achieved by the beam tested at 3.75 x 10^6 cycles. Secondly, from Figure 4.8 it can be seen that the beams tested at 1 x 10^6 and 2.4 x 10^6 cycles show hardly any stiffness reduction. However for the beam tested at 3.75 x 10^6 cycles, there is a significant reduction in stiffness through fatigue induced effects. This beam corresponds to the region in Figure 4.3 where the stiffness is starting to be rapidly lost.

4.2.3 S-N Curve

A typical S-N curve is usually a plot of stress against number of cycles. For convenience and better visual presentation, the applied load has been plotted against LogN. However the shear stress can easily be calculated from Equation 3.8

The resulting S-N curve for all the beams tested in Section 4.1 a&b (ie. linear foam cores), show an appreciable amount of scatter. The beams tested at the three frequencies are shown in Figure 4.9 a,b,c.

It was decided to initially 'eyeball' in a line of best fit through the fatigue data. The slopes (gradient = tanθ) of the lines were then measured for each of the three frequencies (see Figures 4.9 a,b,c) for comparison purposes. From the slopes, no discernible trend could be noted using only the three frequencies. Further testing at other frequencies and using proper regression techniques should yield meaningful trends.

When finding the average y-intercept depicting the load at zero cycles (i.e static ultimate load), it was found the mean load was 12.1 N/mm (8.8 psi) which corresponds exactly with the value of 12.1 N/mm (8.8 psi) given by static testing in Section 3.3.1. This seems to point to the fact that a line is an appropriate fit to the S-N data.

The fatigue scatter present in this case can in the main be attributed to the following :

- variation in material properties
- variation in testing conditions (eg. temperature)
- variation in applied load
- validity of the fatigue rig itself

In terms of variables which are readily available to the designer, these are nominal load, core density and testing frequency.

A) Effect of core density

It was thought that the variability of material properties, namely core density, could be the main cause of scatter. When manufactured, each panel (of known measured core density) is cut into four beams. It is therefore assumed that all beams from the same panel have the same density. In practice this may not be the case as core properties can vary within a panel. However for practical purposes an average value must be used. The core density, shown by quality control sheets when manufactured, did vary significantly despite being assigned a nominal value. For the beams tested (nominal value 80 kg/m^3), the standard deviation of core density for a mean value of 83.58 Kg/m^3, was found to be 4.44 Kg/m^3 or 5.31%. Over the whole range of core densities, the maximum difference was found to be 14.1 Kg/m^3 or 16.9%.

An attempt to largely eliminate the effect of core density was made by normalizing the mean load with respect to density. A plot is shown in Figure 4.10. It is seen that the scatter is slightly reduced showing core density has some significance, but still does not have any major effect. However general trends suggest that fatigue life is improved if the core density lies in the upper region of the normal density distribution.

B) Effect of variation in load

A typical load versus number of cycles curve is given in Fig 4.11. It is seen that the applied load is subject to variations over time. In extreme cases for low loading levels (i.e 3.5 psi), the maximum difference from a mean/nominal value of applied load over the entire testing period was found to be about 0.2 psi, a variation of about 6%. This is caused by the limitations of the equipment used in controlling the pressure, since small variations in pressure

(determined by the cut in and cut out levels of the compressor) are not totally eliminated by the use of a gate valve. In order to largely remove this effect, servo-valves could be utilised. Variations in pressure levels, especially for long term testing, can also be due to calibration and variations in room temperature.

Another observation, is that in some instances the beam may move on the rubber pads during testing, altering the load values read on the load transducers, and in some cases dropping low enough to trigger switching off the beam. Means of reducing this effect are being investigated.

Checks have been made on the fatigue lives of beams tested at nominally the same load but with marginally varying actual load profiles to investigate consistent trends. None have been found suggesting that the small variations in loading have not influenced the fatigue lives significantly.

4.2.4 Effect of frequency

Testing at higher frequencies was carried out, primarily to see if testing can be done more quickly (hence saving testing time, without significantly changing the fatigue life). From the S-N curve for variable frequency for linear foam cores (see Figure 4.12), it can be observed that a change of frequency in the range 0.33 to 0.91 Hz, has no noticeable effect on the fatigue life.

The highest frequency that could be achieved on the rig without prematurely cutting off part of the load or unload cycle of the square wave was in fact 0.9 Hz, so the desired frequency of 1.0 Hz could not quite be achieved. This is because even though the loading is idealised as a square wave, the pneumatic rams take a finite time t_l to load, and t_u to unload (see Figure 4.1). The higher the applied the greater the times t_l and t_u. It is conceivable that increased frequencies may induce localised heating effects in the core thereby increasing the amount of creep per cycle. Further investigation needs to be carried out about the significance of such frequency effects. A suitable method might include placing thermocouples in the core material itself and/or using thermograph techniques.

4.3 Application to High Density Cross-Linked Airex (R90.200) Foam

4.3.1 Deflection - No. of Cycles curve

A typical deflection versus number of cycles plot is shown in Figure 4.13, and shows that the cross-linked foam behaves very similarly to linear foam except that there is no stage of accelerating deflection before failure as the failure is catastrophic in nature. A more detailed description on the failure mode is given in the next section.

The deflection curve shows an overall increase in deflection with two distinct stages. The first stage is that of increasing deflection but rapidly decelerating until the second stage where a slow constant rate of increasing deflection is reached. This constant rate of deflection or creep, is typically slower than for linear foam. This is to be expected since cross-linking forms a much more rigid material structure making it less creep sensitive. Figure 4.14 shows the change in stiffness of the beam during fatigue cycling. It can be seen that stiffness drops at a constant rate until catastrophic failure.

4.3.2 Failure Mode

Testing of the cross-linked foams is still in its early stages and as yet the S-N curve is not fully defined. The failure mode is the same as for both the experimental static testing outlined in Section 3.4.1 and the theoretical failure mode predicted in Section 3.4.3. All the failures have occurred at the beams midspan (650mm from either support) on the thinner tensile facing, where the bending moment is greatest. The failure mode is that of tensile failure of the skin due to fatigue loading with no permanent distortion by core yielding visible. The exact point of failure can be predicted after the test has been running for some time, by a white streak dividing the beam in half, on the tensile facing. This whitening preceding fatigue failure is typical of many GRP structures. The failure in this case is catastrophic since once the tensile skin fails, the beam suddenly loses most of its flexural rigidity. The core instantly has to carry a vastly increased tensile loading and fails instantly by cracking along the line of the skin failure. Delamination of skin from core also follows as the beam suddenly deflects on failure. The complete

failure process takes a fraction of a second and is accompanied by an extremely loud bang (similar to a gun going off). A detailed description of the failure mechanisms is given in Section 2.3.1. Because the failure is so rapid, the deflection curve shows no sign of accelerating deflection in the final stages. With lower loads such (i.e 10 psi), it has been observed that small amounts of cracking have taken place in the core before skin failure, by propagating from the tensile face/adhesive interface joint, towards the centre of the core. In each case core cracking only starts after significant cycling (in the order of 400 000 or more cycles), and propagates from the skin where whitening is observed. However each point of skin failure for the 10 psi cases have been off centre but still within the region between the two middle rams where the bending moment is constant and a maximum.

4.3.3 S-N curve

The S-N curve for the cross-linked foam (Figure 4.15), shows significantly reduced amounts of scatter when compared to the linear foams. The slope of the S-N curve for the Airex R90.200 foam is much greater than for linear foams as it has a greater shear strength. As for linear foams, the ultimate static strength predicted from the y-intercept (i.e at zero cycles), of 39.0 N/mm (28 psi) is in line with the expected value of independent static testing.

Det Norske Veritas (DNV) has been doing some research on sinusoidal and slamming fatigue and they have compared various foam cores, namely Divinycel H100, H200 and Airex R63.80 (56). It was found that fatigue data for both slamming and sinusoidal loading for the same core material coincided on the same S-N curve (see Figure 4.16a). Additionally it was found that when the maximum shear stress was normalised with respect to the static linear limit point (yield point) shear stress of the core material then all the data for different foam cores also fits one S-N curve (see Figure 4.16b). However it is very important that the proper yield point of the core material is obtained as described earlier when predicting the static failure mode. For the cross-linked foam as described in Section 3.4.3, the 'yield' shear stress was taken as 3.0 N/mm^2 because the failure mechanism is skin failure. A S-N curve comparing the maximum shear stress of both the linear and the cross-linked foam both tested at the same frequency is shown in Figure 4.17a. However when normalising the data with respect to the static linear shear stress limit of

the core, the two plots do not lie on the same S-N curve as reported from findings by DNV (see figure 4.17b). It is interesting to note that DNV used a shear stress value of 2.4 N/mm^2 for Divinycel H200 foam which from Figure 3.1 shows similar performance to Airex R90.200. Divinycel H200 has a higher shear modulus so it is arguable that its shear stress yield point will also be slightly higher than Airex R90.200. However no precise conclusions can be made until further testing of the foam is undertaken.

Again, as for linear foams the amount of scatter can be explained in terms of the effect of core density and the variation in applied load.

4.3.4 Effect of Density

The densities of the higher density core material were gained from the sandwich panel manufacturers quality control sheets as for the linear foams stated previously. For the beams tested (nominal value of 200 Kg/m^3), the standard deviation for a mean value of 200.85 Kg/m^3 was 8.83 Kg/m^3 or 4.4%. The maximum difference in densities was 28.4 Kg/m^3 or 14%. This may seem large but in percentage terms the variation of core densities is in fact slightly less than for the linear foam.

In this case it was not expected that core density would be an important parameter because failure was associated with the facings and not the core. This may be one reason why the scatter is much reduced because the large variability in core density do not have to be accounted for.

4.4 Discussion

In summary, the amount of scatter observed on the S-N curve for the two foams seems to be largely linked to one of two factors or indeed an interaction of both. These are the dependence of core density on the failure mechanism and the variation of applied load as a percentage of the mean load. However it seems very probable that the small variation of skin properties (not measured) and the lack of control of room temperature during testing may contribute to a small amount of scatter.

For low density linear foams under cyclic loading, the failure mechanism was core shear which means that core material properties become very important when evaluating fatigue life. For the higher density cross-linked foam the failure mechanism was skin failure hence skin material properties are the dominant factor in determining fatigue life.

It is also imperative that accurate data for material properties are obtained and that manufacturers data should be used with extreme caution.

5.0 Concluding Remarks

This report has sought to address three issues :

Firstly, a wide-ranging background study has been conducted covering issues related to material characterisation, sandwich beam/panel behaviour under static loads, creep performance under sustained static loading and fatigue behaviour of FRP laminates as well as sandwich configurations.

Secondly, a comprehensive characterisation of sandwich beams, covering theoretical and experimental aspects, has been outlined. The theoretical calculations have covered the contributions of the skins and the foam core material.

Thirdly, results pertaining to fatigue tests on FRP sandwich beams with two different foam types have been outlined. The tests have covered the impact of varying frequencies. These will form the basis of further evaluation of damage accumulation and fatigue life prediction.

6.0 References

1 **O.Gullberg, K.A Olsson**
Design & Construction of GRP Sandwich Ship Hulls
Maritime Structures, vol 3, No. 2, 1990

2 **R.P Reichard**
Enhanced Shock Performance Of FRP Sandwich Structures
1st Int Conf on Fast Sea Transportation, Trondheim, June 1991
Vol 1, pp 399-411

3 **2nd Int Conf on Sandwich Construction**
University of Florida, Gainesville, Florida, U.S.A
Volumes 1&2, March 9-12, 1992

4 **E.T Moyer, G.G Amir, K.A Olsson, S.E Hellbratt**
Response of GRP Sandwich Structures Subjected to Shock Loading
Vol 1, loc cit 4.

5 **K.A Olsson, A.Lonno**
Sandwich Constructions - Recent Research & Development
Second Int Conf on Sandwich Construction
Vol 2, Florida, USA, March 1991

6 **L.N Phillips (ed)**
Design with Advanced Composite Materials
The Design Council, London, 1989
ISBN: 0-85072-238-1

7 **R.A Shenoi, J.F Wellicome (ed)**
Composite Materials in Maritime Structures
Cambridge Ocean Technology Series
Cambridge University Press, 1993
Vol 1: ISBN: 0-521-45153-1
Vol 2: ISBN: 0-521-45154-X

8 **F.D Hudson**
Composites in a New Generation of Lifeboats
British Plastics Federation Conference on Composites
Manchester, Oct, 1990

9 **C.S Smith**
Design of Maritime Structures in Composite Materials
Elsevier Applied Science, London, 1990
ISBN: 1-85166-416-5

10 **D Hull**
A Revolution in Materials : Fibre Composites
The North East Coast Institution Of Engineers And Shipbuilders
Vol 106, Part 1, 1989

11 **P.W.R Beaumont**
The Failure of Fibre Composites : An Overview
Journal of Strain Analysis, Vol 24, No. 4, 1989

12 **G Lubin (ed)**
Handbook of Composites
SPE monograph series
Van Nostrand Reinhold, New York, 1982
ISBN: 0442248970

13 **E Greene**
Sandwich Construction
Ship Structure Committee
Use of Fibre Reinforced Plastics in Marine Structures
Sept 6, 1990

14 **H.T Hahn**
Non-linear Behaviour of Laminated Composites
Journal of Composite Materials, Vol 7, April, 1973

15 **L.J Broutman, B.D Agarwal**
Analysis and Performance of Fibre Composites
John Wiley & Sons Inc, 1990
ISBN: 0-471-51152-8

16 **H.G Allen, K Raybould**
High Performance Composites and their Effectiveness in Sandwich Panels.
6th Int High Speed Surface Craft Conf, London, Jan, 1988

17 **G Caprino, R Teti**
Sandwich Structures Handbook
Il Prato, April, 1989

18 **E Gellhorn, G Reif**
Think Dynamic- Dynamic Test Data for the Design of Dynamically Loaded Structures
Vol 2, loc cit 3

19 **H.G Allen**
Analysis & Design of Structural Sandwich Panels
Pergamon Press, London, 1969
ISBN: 08-012869-8

20 **H.G Allen**
Theory of Sandwich Beams & Plates
Composite Materials in Maritime Structures
Vol 1, p. 205-235, loc cit 7

21 **J.C.M Theulen, J.M Peijs**
Optimisation of Bending Stiffness & Strength of Composite Sandwich Panels
Composite Structures, Elsevier Science Publishers, 1990

22 Sandwich Panels under Normal Loading
Structures Sub Series - Vol 9
Engineering Sciences Data Unit, 1977

23 J.F Davalos, E.J Barbero, Y.Kim
A 2-D Laminated Beam Finite Element with Layer Wise Constant Shear
Vol 1, loc cit 3

24 A.Starlinger, F.G Rammerstorfer
A Finite Element Formulation for Sandwich Shells Accounting for Local Failure Phenomena
Vol 1, loc cit 3

25 Zheng-Chang Liu
Finite Element Analysis of Sandwich Plates
Vol 1, loc cit 3

26 Y Rothschild, A.T Echtermeyer
Simulation of Yield & Plastic Flow of 3-D Sandwich Foam Cores
Vol 1, loc cit 3

27 R Damonte
Finite Element Analysis for Composites
Composite Materials in Maritime Structures
Vol 1, p. 255-279, loc cit 7

28 G.D Sims
Test Procedures and Standards
Composite Materials in Maritime Structures
Vol 1, p. 316-339, loc cit 7

29 H.G Scholte
Fatigue Characteristics
Composite Materials in Maritime Technology
Vol 2, p. 178-196, loc cit 7

30 R Talreja
Fatigue of Composite Materials
Technomic Publishing Company, Pennsylvania, 1987

31 P.T Curtis
The Fatigue Behaviour of Fibrous Composite Materials
Journal of Strain Analysis, vol 24, 1989

32 S.L Ogin
Fatigue in Composite Materials
Composite Materials Technology, University of Surrey
July, 1991

33 K.L Reifsnider, A Talug
Analysis of Fatigue Damage in Composite Materials
Int Journal of Fatigue, Jan 1980

34 C.C Osgood
Fatigue Design.
Int Series on Strength & Fractuer of Materials & Structures
Pergamon Press, 1982
ISBN: 0-08-026166-3

35 **P.T Curtis**
Theoretical Predictions of Failure Mechanisms and Strength
Composite Materials in Maritime Structures
Vol 1, p. 280-305, loc cit 7

36 **L.J Broutman, S Sahu**
A New Theory to Predict Cumulative Fatigue Damage in Fibre Reinforced Plastics
Composite Materials : Testing and Design (2nd Conf), ASTM STP 497, 1972, pp 170-188

37 **H.T Hahn, R.Y Kim**
Proof Testing of Composite Materials
Journal of Composite Materials, Vol 9, 1975

38 **A Charewicz, I.M Daniel**
Damage Mechanisms and Accumilation in Graphite/Epoxy Laminates
Composite Materials : Fatigue & Fracture, H.T Hahn (ed), ASTM STP 907, 1986, pp 274-297

39 **H.B Hwang, K.S Han**
Fatigue of Composite Materials : Damage Model & Life Prediction
Composite Materials : Fatigue & Fracture, (2nd Conf), P.A Lagace (ed)
ASTM STP 1012, 1989, pp 87-102

40 **B Hayman, O.E Sund**
Shear Properties of GRP Sandwich Beams Subjected to Slamming Loads
Vol 2, loc cit 3

41 Standard Test Method for Shear Fatigue of Sandwich Core Materials. C394-62
ASTM Standards and Literature References for Composite Materials, ASTM pp 149-150, 2nd edition, 1990

42 **L Buene, A.T Echtermeyer, O.E Sund, M.K Nygard, B Hayman**
Assessment of Long Term Effects of Slamming Loads on FRP Sandwich Panels
1st Int Conf on Fast Sea Transportation, Trondheim, June, 1991
vol 1, pp 365-379

43 **D Weissman-Berman**
Visco-elastic Response of Sandwich Beams
Vol 1, loc cit 3

44 **H Kraus**
Creep Analysis
Wiley Interscience, 1980
ISBN: 0-471-06255-3

45 **J Gittus**
Creep, Viscoelasticity & Creep Fracture in Solids
Applied Science Publishers Ltd, 1975
ISBN: 0-85334-597-X

46 **J.T Boyle, J Spense**
Stress Analysis for Creep
Butterworths, 1983
ISBN: 0-408-01172-6

47 **A.I Smith, A.M Nicholson (ed)**
Advances in Creep Design
Applied Science Publishers Ltd, 1971
ISBN: 0444-20119-X

48 **Yu.N Rabotrov**
Creep Problems in Structural Members
North Holland Publishing Company, 1969
ISBN: 7204-23570

49 Inelastic Behaviour of Composite Materials
AMD- vol 13, C.T Herakovich (ed), ASME Winter Annual Meeting,
Houston, Texas, U.S.A, Nov 30 - Dec 5, 1975

50 **D.A Dillard, D.H Morris, H.F Brinson**
Predicting Viscoelastic Response and Delayed Failures in General
Laminated Composites
Composite Materials : Testing & Design (6th Conf), I.M Daniel (ed),
ASTM STP 787, 1982, pp 357-370

51 **U. Korin**
Creep Superposition Principle.
Dept of Civil Engineering PHD
University of Southampton, 1969

52 Standard Test Method for Flexure Creep of Sandwich Constructions. C480-62
ASTM Standards and Literature References for Composite Materials
ASTM 2nd edition, 1990
ISBN: 0-8031-1230-0

53 **S Burkhardt**
Newer Investigation into Load Bearing Behaviour of Sandwich Elements
First Int Conf on Sandwich Constructions
Stockholm, June 1989

54 **J.L Chevalier**
Creep & Fatigue Properties of End-Grain Balsa and other Typical Sandwich
Cores
Vol 2, loc cit 3

55 **K.G Folke**
Mathematical Theory of Creep & Creep Rupture
Clarendon Press, 1966

56 **B Hayman, T Haug, S Valsgard**
Response of Fast Craft Hull Structures to Slamming Loads
1st Int Conf on Fast Sea Transportation, Trondheim, June 1991
vol 1, pp 381-389

57 **H.G Allen, R.A Shenoi**
Flexural Fatigue Tests on Sandwich Structures
Vol 2, loc cit 3

58 **R.A Shenoi, S. Aksu, H.G Allen**
Fatigue Characteristics of FRP Sandwich Beams
Int Journal of Fracture and Fatigue of Engineering Materials and Structures
(Accepted for publication : To appear)

59 **A.J Munday, R.A Farrar (ed)**
An Engineering Data Book
Macmillian Education Ltd, 1979
ISBN : 0-333-25829-0

60 Airex Sandwich Technology data sheets
Airex R90 Rigid high Density Foam
Airex R63 Tough Rigid Foam
Airex AG speciality Foams CH-5643 Sins
Phone (+41) 42/66 0066

61 Fast Carriage Boat Testing Programme Results
Technical Report TR 354
SP Technologies, Isle of Wight, 1990

7.0 Acknowledgements

The work outlined in this report has been funded under the DTI / SERC Link Structural Composites Programme. The authors wish to acknowledge the financial support of DTI, SERC and the RNLI. The authors have also benefited considerably from regular discussions with Mr I.A Hicks, Technical Manager of RNLI.

TABLES

Table 3.1 Properties of Facings Material (source - Reference 58)

Constituent	Property	Value
	thickness	3.0 mm
Top Skin	Young's modulus	14.7 KN/mm^2
	tensile strength	181.0 N/mm^2
	thickness	5.5 mm
Bottom Skin	Young's modulus	18.2 KN/mm^2
	tensile strength	238.3 N/mm^2

Table 3.2 Properties of Airex Core Materials (source - Reference 60)

Foam Type	Property	Value
	thickness	50 mm
	nominal density	80 Kg/m^3
Airex R63.80	Young' modulus	64.0 N/mm^2
	shear modulus	21.0 N/mm^2
	shear strength	1.2 N/mm^2
	thickness	50 mm
	nominal density	200 Kg/m^3
Airex R90.200	Young's modulus	194.0 N/mm^2
	shear modulus	70.0 N/mm^2
	shear strength	3.0 N/mm^2

Table 4.1a : Sandwich Beam Experimental Fatigue Results
(* indicates faint cracking)

AIREX R63.80 Foam Core
Frequency = 0.33 Hz

Beam number	rig number	Applied load (psi)			deflection (mm) (elastic)		failure		
		Nominal	actual				deflection limit (mm)	number of cycles	type
			mean+	sd+	mean#	sd#			
1	0	5.0	5.219	0.244	16.980	1.379	60.0	36076	plastic
2	1	5.0	4.990	0.097	20.260	1.962	60.0	10481	plastic
3	2	5.0	5.168	0.156	18.613	1.557	60.0	23268	cracking*
5	1	5.0	4.990	0.067	22.761	5.847	60.0	1239	cracking*
6	2	5.0	5.203	0.102	22.791	4.281	60.0	906	plastic
7	0	5.0	5.402	0.186	23.980	3.172	60.0	531	plastic
8	0	5.0	5.199	0.107	21.327	3.084	60.0	1780	plastic
9	1	5.0	4.749	0.197	18.351	2.260	60.0	19357	cracking*
10	2	5.0	5.044	0.084	21.607	3.329	60.0	1867	plastic
13	2	4.0	4.355	0.131	16.216	4.185	60.0	2428	plastic
14	0	4.0	4.054	0.132	15.789	1.479	60.0	5210	plastic
15	1	4.0	3.708	0.170	16.259	6.609	60.0	2535	plastic
16	0	4.0	3.786	0.191	12.955	1.666	60.0	55973	plastic
17	1	4.0	3.917	0.124	16.022	5.004	60.0	11940	plastic
18	2	4.0	3.898	0.179	15.352	1.507	60.0	28526	plastic
19	0	4.0	3.888	0.449	8.224	6.811	60.0	202167	plastic
20	1	4.0	3.845	0.299	14.276	1.458	60.0	262215	cracking
21	2	4.0	3.883	0.319	13.960	1.046	60.0	228850	cracking
22	0	6.5	6.365	0.282	24.159	2.553	80.0	1111	plastic
23	0	3.5	3.528	0.345	13.069	1.685	60.0	717830	cracking
24	1	3.5	3.441	0.094	12.854	1.905	60.0	22296	plastic
25	2	3.5	3.508	0.189	19.591	9.550	60.0	7013	plastic
26	1	3.5	3.548	0.163	13.454	0.918	60.0	475791	plastic
27	2	3.5	3.506	0.184	14.885	4.436	60.0	402780	cracking
28	0	3.5	3.518	0.327	11.867	0.667	60.0	781113	cracking
29	0	6.0	6.226	0.140	24.386	2.806	80.0	1004	plastic
30	1	6.0	5.892	0.229	31.559	6.638	80.0	590	plastic
31	2	6.0	5.887	0.229	27.193	3.777	80.0	714	plastic
32	0	6.5	6.501	0.114	24.090	3.354	80.0	1445	plastic
33	1	6.5	6.476	0.283	29.691	6.034	80.0	1350	cracking*
34	2	6.5	5.932	0.708	33.795	4.043	80.0	433	cracking
35	0	6.5	6.443	0.040	27.750	3.862	70.0	576	plastic
36	1	6.5	6.312	0.239	28.258	7.428	70.0	1204	plastic
37	2	6.5	6.192	0.407	28.095	5.911	70.0	937	plastic
38	1	2.5	-	-	-	-	-	3750000	
39	1	2.5	2.541	0.142	9.212	0.626	-	2359733	
40	2	2.5	2.464	0.176	10.715	0.608	-	1027694	
41	2	5.5	-	-	-	-	-	688	cracking*
42	2	5.5	5.209	0.148	25.916	2.456	60.0	2271	cracking*
43	2	5.5	5.316	0.094	24.974	3.911	60.0	901	cracking*
44	2	4.0	4.080	0.143	17.575	2.361	60.0	39233	plastic

Table 4.1b : Sandwich Beam Experimental Fatigue Results

AIREX R63.80 Foam Core
Frequency = 0.50 Hz

Beam no.	Rig no.	Density (kg/m^3)	Applied Load (psi) Nom	actual Mean	actual sd	Deflection (mm) Mean	Deflection (mm) sd	No. Cycles	Max Distortion (mm)
45	1	-	3.5	3.789	.138	14.42	1.09	184350	73
46	0	-	3.5	3.704	.136	16.37	3.10	14540	70
47	1	-	4.5	4.482	.101	20.63	5.43	2226	73
48	0	-	4.0	4.003	.156	13.91	1.28	351248	79
49	1	-	4.5	4.500	.048	16.38	1.69	47760	74
50	0	-	4.5	4.613	.121	16.73	0.88	184514	70
51	1	-	5.5	5.601	.043	23.19	3.05	2251	67
52	2	-	5.0	4.835	.203	21.35	2.25	17454	70
1a	1	74.8	5.5	5.843	.136	24.43	2.54	451	73
1b	2	74.8	3.5	3.519	.156	14.83	0.98	182556	96
1c	0	74.8	4.5	4.443	.152	16.64	1.11	104361	84
1d	1	74.8	5.5	5.586	.080	24.96	2.24	401	74
2c	2	76.2	3.5	3.609	.293	15.61	3.42	39938	69
2d	1	76.2	3.5	3.665	.159	15.03	0.86	86499	90
4a	2	81.8	3.5	3.439	.136	15.03	0.50	180836	77
4b	0	81.8	4.5	4.663	.066	16.86	0.93	20525	84
4c	2	81.8	3.5	3.469	.036	14.12	0.69	527849	70
4d	1	81.8	5.5	5.644	.110	25.80	2.36	602	89
5a	0	82.8	3.5	3.441	.111	13.84	0.77	84058	95
5d	0	82.8	4.5	4.499	.068	16.64	1.14	11601	91
13b	0	87.8	5.5	5.577	.073	21.94	1.62	1353	79
13d	1	87.8	5.5	5.512	.050	24.95	2.70	651	-

Table 4.1c : Sandwich Beam Experimental Fatigue Results

AIREX R63.80 Foam Core
Frequency = 0.91 Hz

Beam No.	Rig No.	Density (Kg/m^3)	Applied Load (psi) Nom	Actual Mean	Actual sd	Deflection (mm) Mean	Deflection (mm) sd	No. Cycles	Max Distortion (mm)
3a	0	79.5	4.5	4.422	0.129	19.30	2.64	5092	89
3b	0	79.5	3.5	3.553	0.107	16.97	1.27	29616	87
3c	1	79.5	4.5	4.558	0.130	17.86	2.05	10755	92
3d	2	79.5	4.5	4.713	0.055	18.10	2.31	13954	70
5b	2	82.8	4.5	4.687	0.188	21.50	3.06	2855	76
5c	0	82.8	3.5	3.529	0.091	13.74	1.06	67242	101
11b	2	83.8	3.5	3.426	0.134	12.18	0.94	331638	116
11c	0	83.8	3.5	3.502	0.107	20.91	2.38	6101	104
12a	0	88.9	3.5	3.695	0.190	13.77	0.59	643891	72
13a	1	87.8	3.5	3.707	0.120	12.17	2.20	411560	81
14b	1	87.5	4.5	4.628	0.075	18.51	1.50	14101	84
14c	0	87.5	4.5	4.613	0.109	18.71	1.33	13084	81
14d	2	87.5	5.5	5.644	0.055	25.92	2.22	1176	73
15b	1	86.7	5.5	5.569	0.100	21.90	3.23	2147	79
15c	0	86.7	5.5	5.688	0.074	25.22	2.20	1151	79
15d	2	86.7	5.5	5.597	0.149	21.61	1.845	2726	68
16a	2	86.1	5.5	5.702	0.082	24.70	2.99	1226	78
16d	1	86.1	5.5	5.629	0.113	24.60	2.76	1127	74

Table 4.2 : Sandwich Beam Experimental Fatigue Results

AIREX R90.200 Foam Core
Frequency = 0.50 Hz

Beam No.	Rig No.	Density (Kg/m^3)	Applied Load (psi) Nom	Actual Mean	Actual sd	Deflection (mm) Mean	Deflection (mm) sd	No. Cycles
22b	1	-	18.0	17.841	0.348	63.33	0.67	1623
23b	1	-	18.0	17.991	0.127	60.25	1.10	3639
23c	2	-	16.0	16.224	0.122	53.33	0.58	8086
25a	0	187.7	16.0	16.362	0.065	54.29	0.64	10529
25b	1	187.7	18.0	17.911	0.211	64.07	0.24	3823
25c	2	187.7	14.0	13.954	0.122	43.82	0.31	60717
25d	2	187.7	16.0	16.336	0.189	52.84	1.60	15588
26a	1	190.8	12.0	11.967	0.393	42.38	1.48	32019
26b	2	190.8	12.0	12.269	0.133	35.99	1.18	227845
26c	1	190.8	12.0	12.204	0.394	39.89	1.38	76614
26d	0	190.8	14.0	14.305	0.076	47.61	0.741	28425
27a	0	205.4	14.0	14.329	0.320	48.82	0.58	22317
27b	0	205.4	14.0	14.302	0.255	44.07	1.26	50411
27c	0	205.4	14.0	14.338	0.212	44.41	1.71	43042
27d	2	205.4	12.0	12.108	0.214	36.81	0.91	223919
28a	0	203.8	16.0	-	-	-	-	9526
28b	1	203.8	12.0	-	-	-	-	93276
28c	1	203.8	16.0	16.158	0.330	51.63	1.75	9032
28d	2	203.8	12.0	-	-	-	-	162785
29a	0	197.7	16.0	16.186	0.161	48.59	0.28	10980
29c	2	197.7	10.0	10.210	0.212	28.78	1.24	1267662
29d	2	197.7	14.0	14.227	0.094	43.25	0.72	54601
30c	1	196.2	10.0	10.120	0.306	32.19	1.19	717446

FIGURES

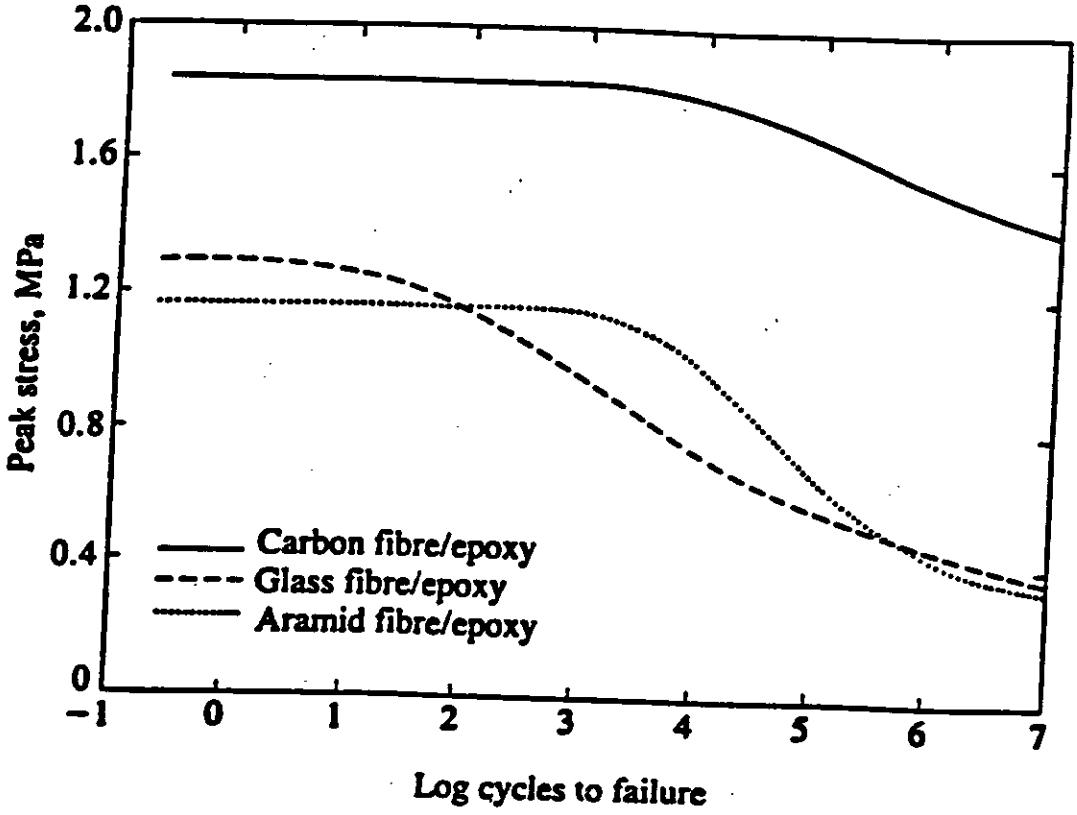

Figure 2.1 **S–N fatigue data for unidirectional composite materials**

Figure 2.2 Typical Fatigue Diagrams

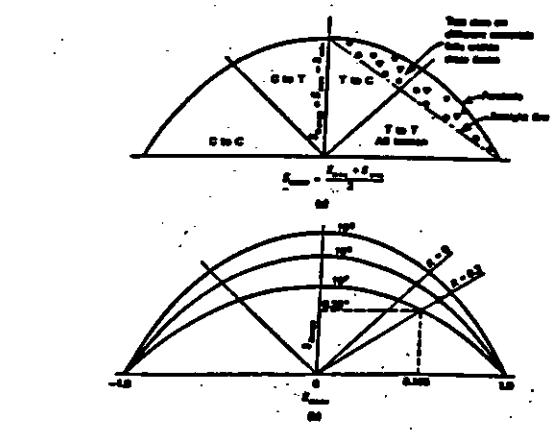

a) $S_a = -0.27 S_m^2 + 0.27$, for 10^7 cycles (for this example)

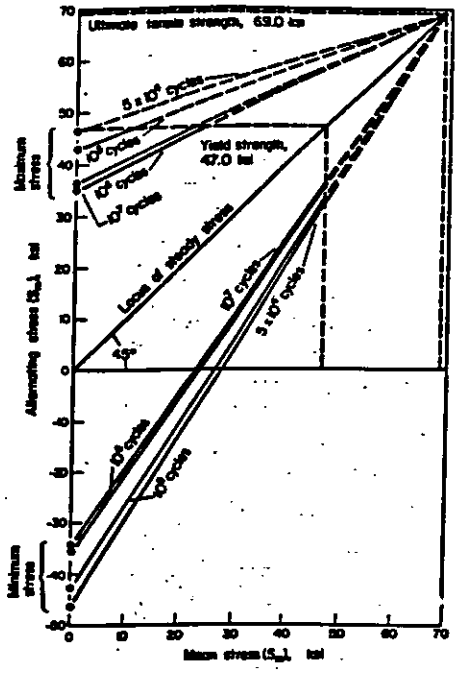

b) Goodman diagram. Modified form (for K-20 steel, as an example).

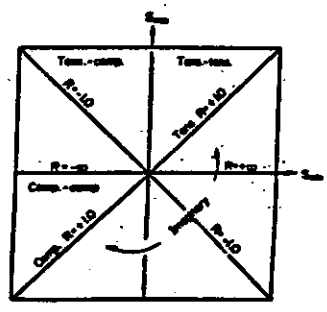

c) Classical Constant-life Diagram.
(a) The Fatigue Square
(b) The Schematic Form
(c) The Conventional Form

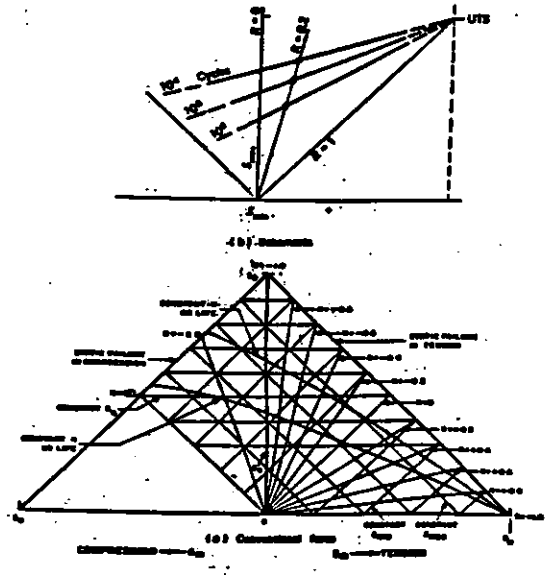

Figure 2.3 : Modes of Core Shear Failure

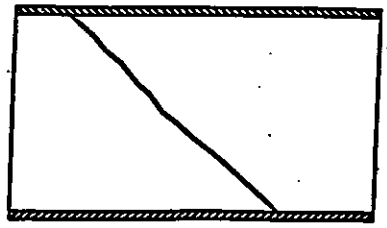

Mode I

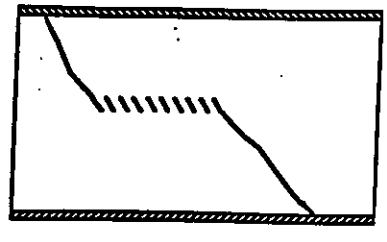

Mode II

Figure 2.4 Typical Creep Curves

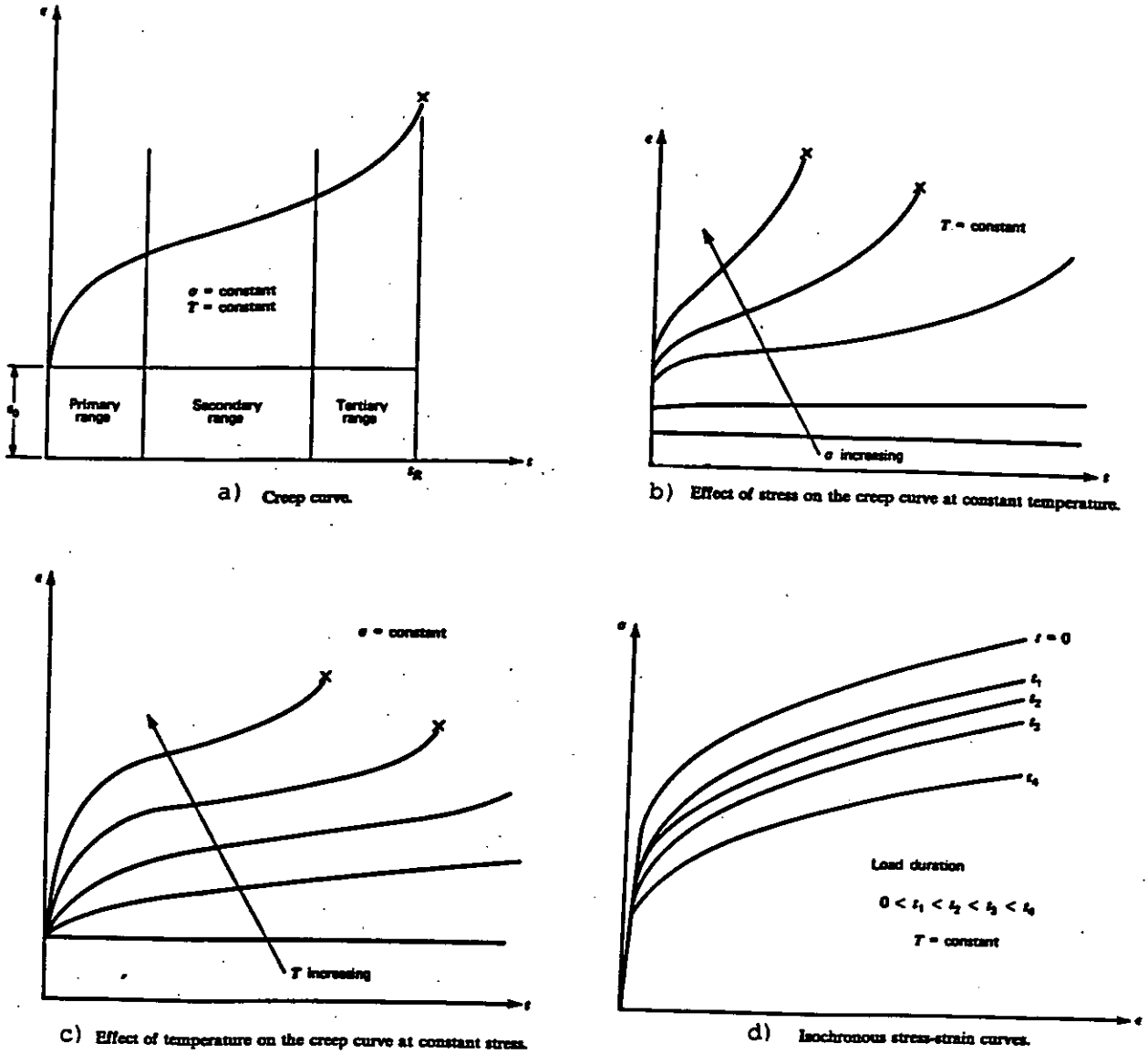

a) Creep curve.

b) Effect of stress on the creep curve at constant temperature.

c) Effect of temperature on the creep curve at constant stress.

d) Isochronous stress-strain curves.

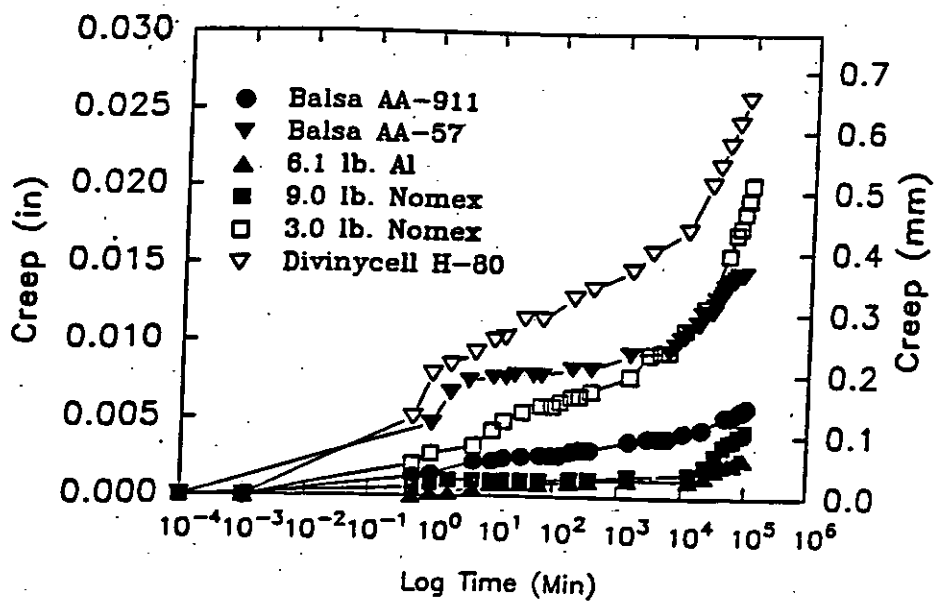

Figure 2.5 Creep Curves for 6 Core Materials

Figure 3.1 LOAD vesus DEFLECTION for Various Beams

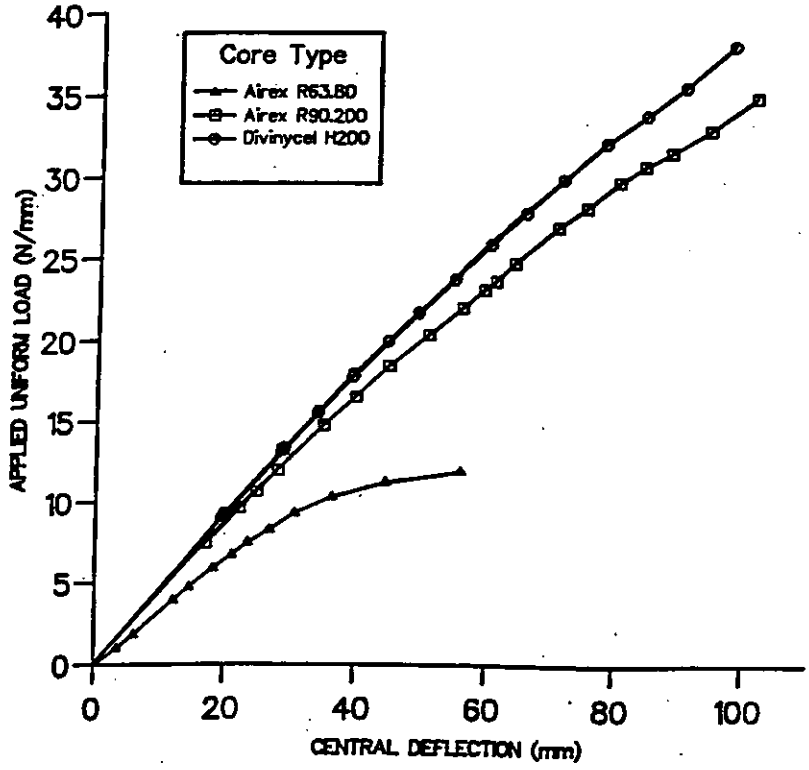

Figure 3.2 Sandwich Beam Dimensions

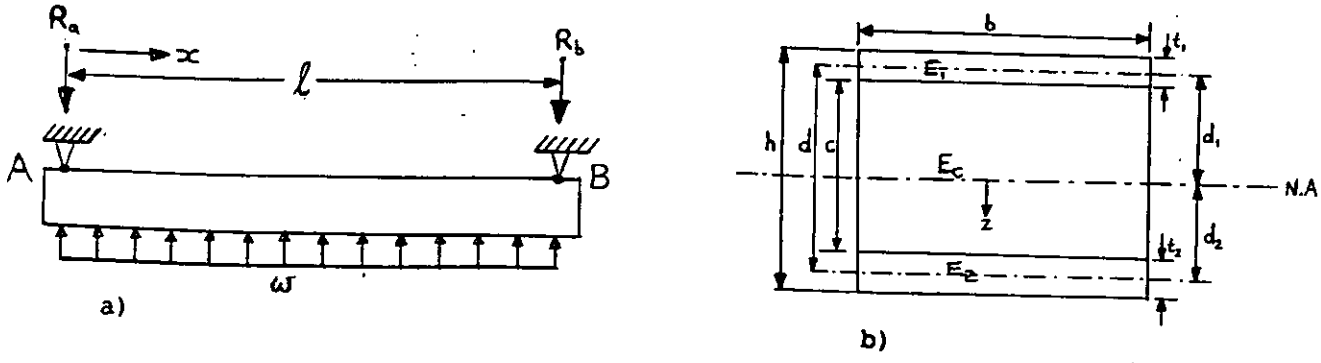

Figure 3.3 Sandwich Beam Configuration

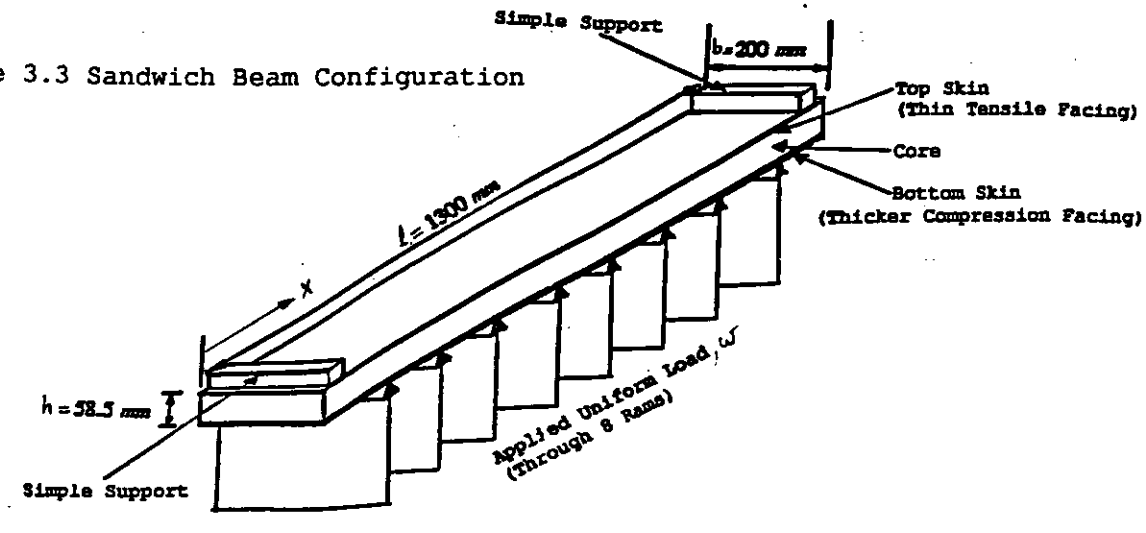

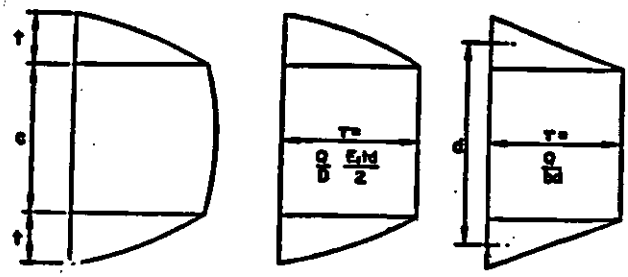

Figure 3.4 Shear stress distribution in sandwich beam.
(a) True shear stress distribution.
(b) Effect of weak core.
(c) Effect of weak core, neglecting the local bending stiffnesses of the faces.

Figure 3.5 Section of Sandwich Beam in Shear

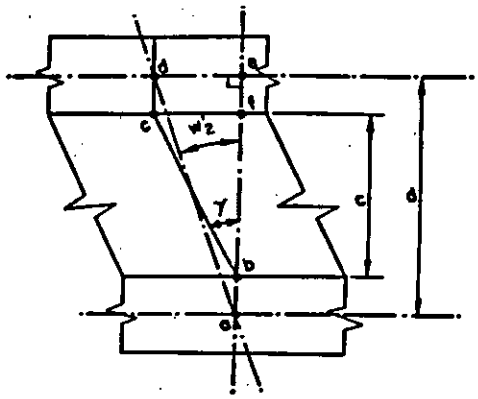

Figure 3.6 INFLUENCE OF BENDING & SHEAR COMPONENTS ON TOTAL DEFLECTION

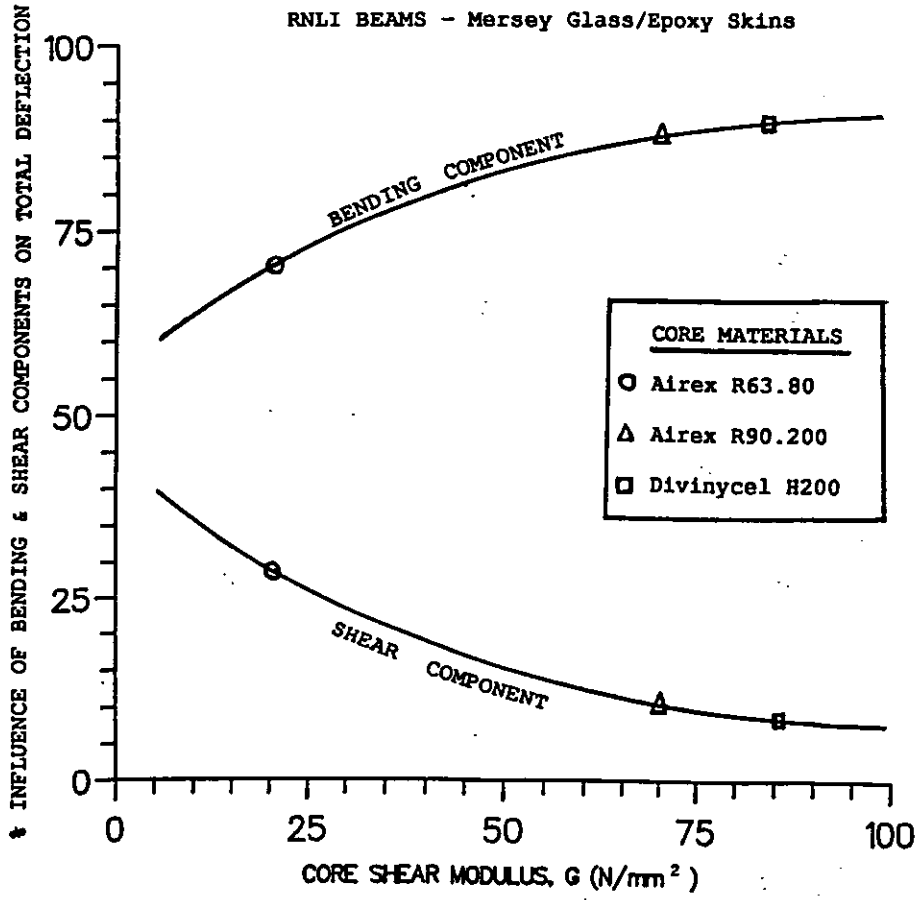

Figure 3.7 Uniform Load versus Deflection for RNLI Sandwich Beam

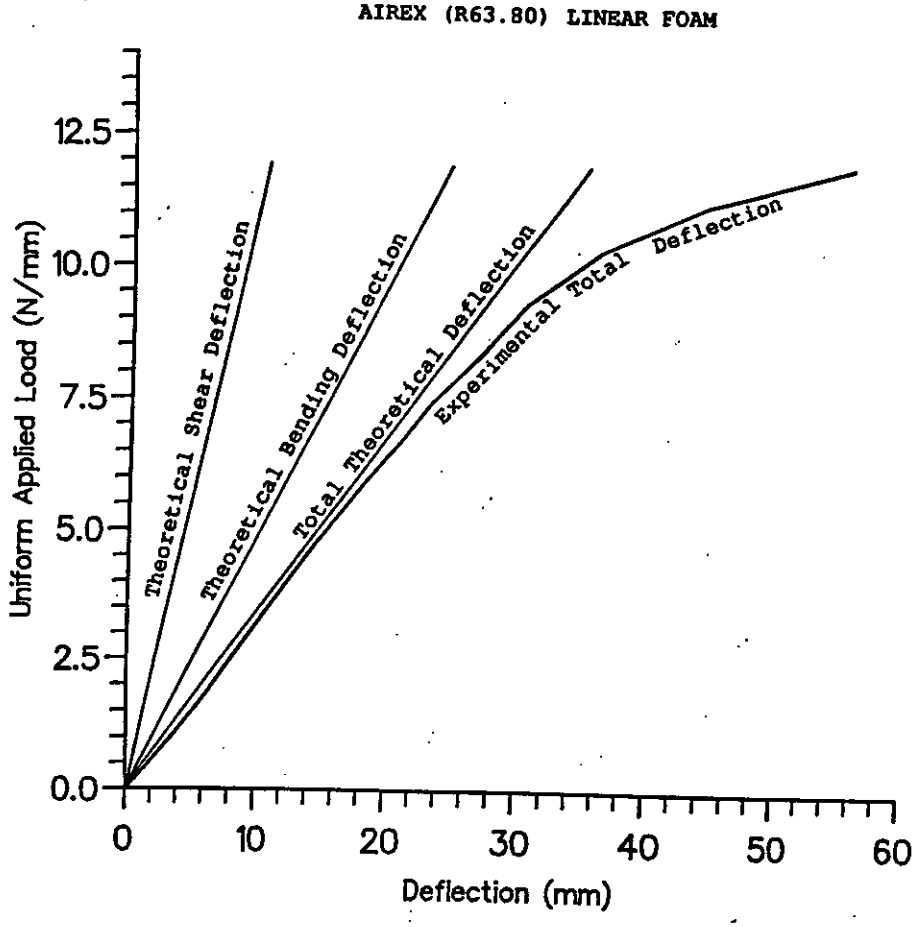

Figure 3.8 STRAIN RATE DEPENDENCE OF R 63.80
Shear Test

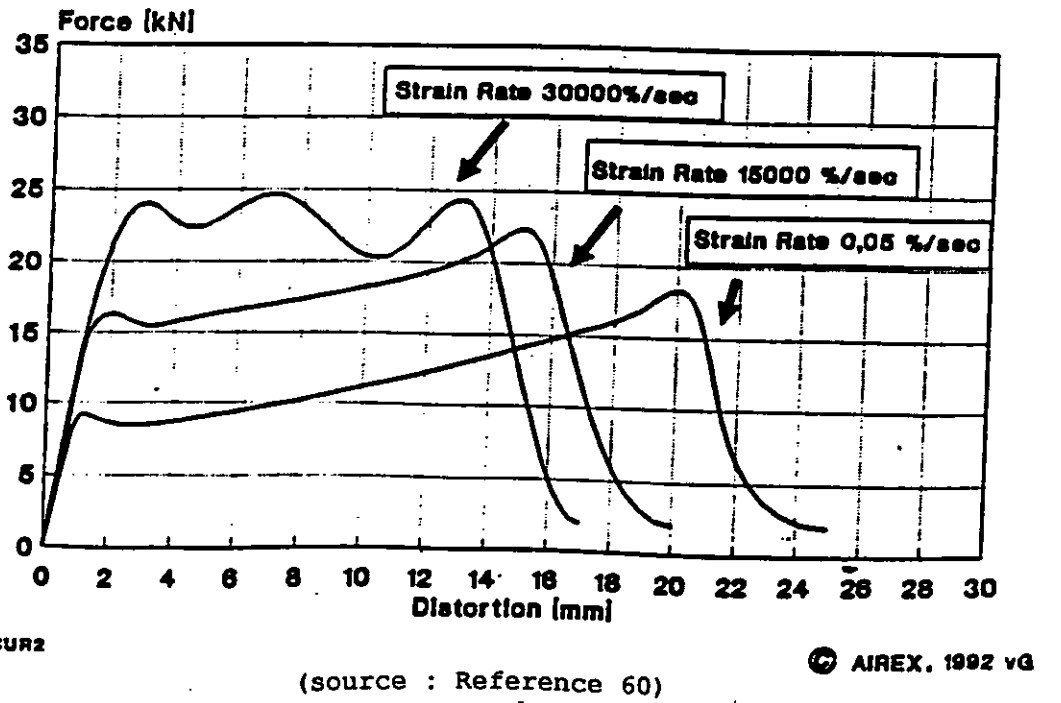

(source : Reference 60)

Figure 3.9 Shear Stiffness versus Deflection for RNLI Sandwich Beam

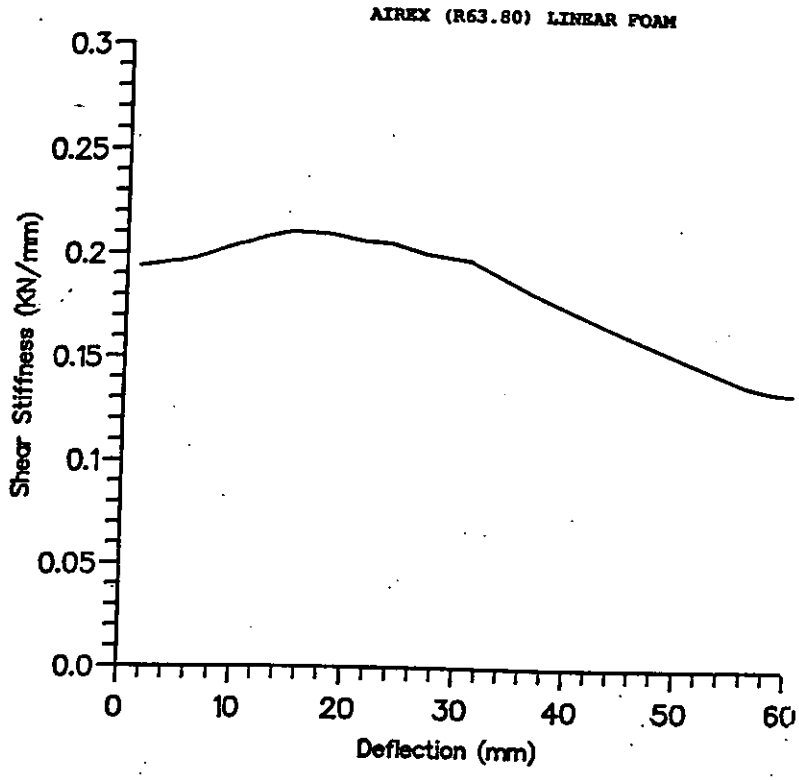

Figure 3.10 Shear Stress in Core

a) **Shear stress in core (uniformly-distributed load)**

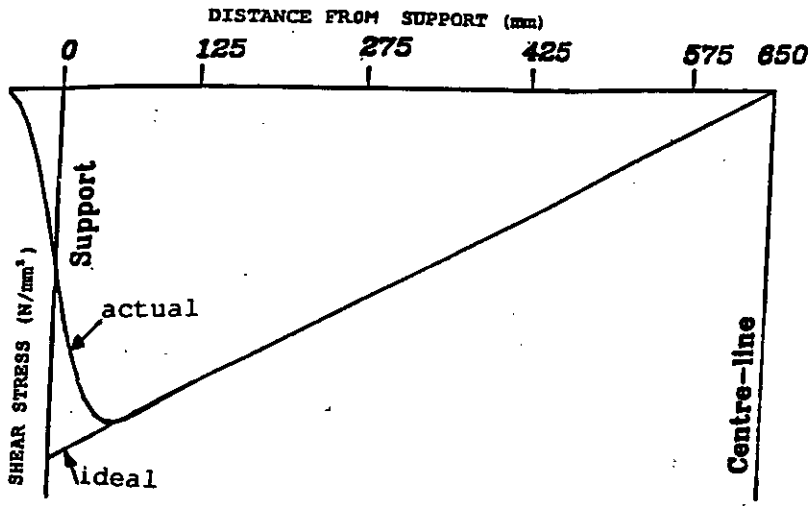

b) **Shear stress in core (eight equal point loads)**

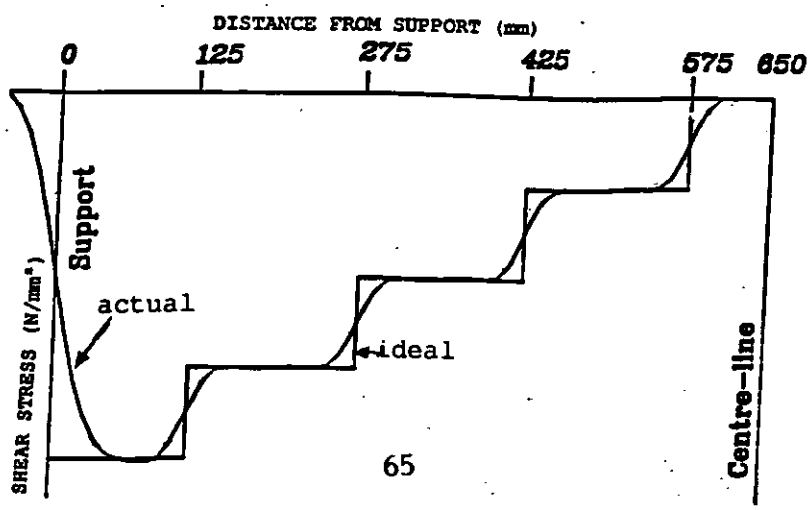

Figure 3.11 Uniform Load versus Defection for RNLI Sandwich Beam

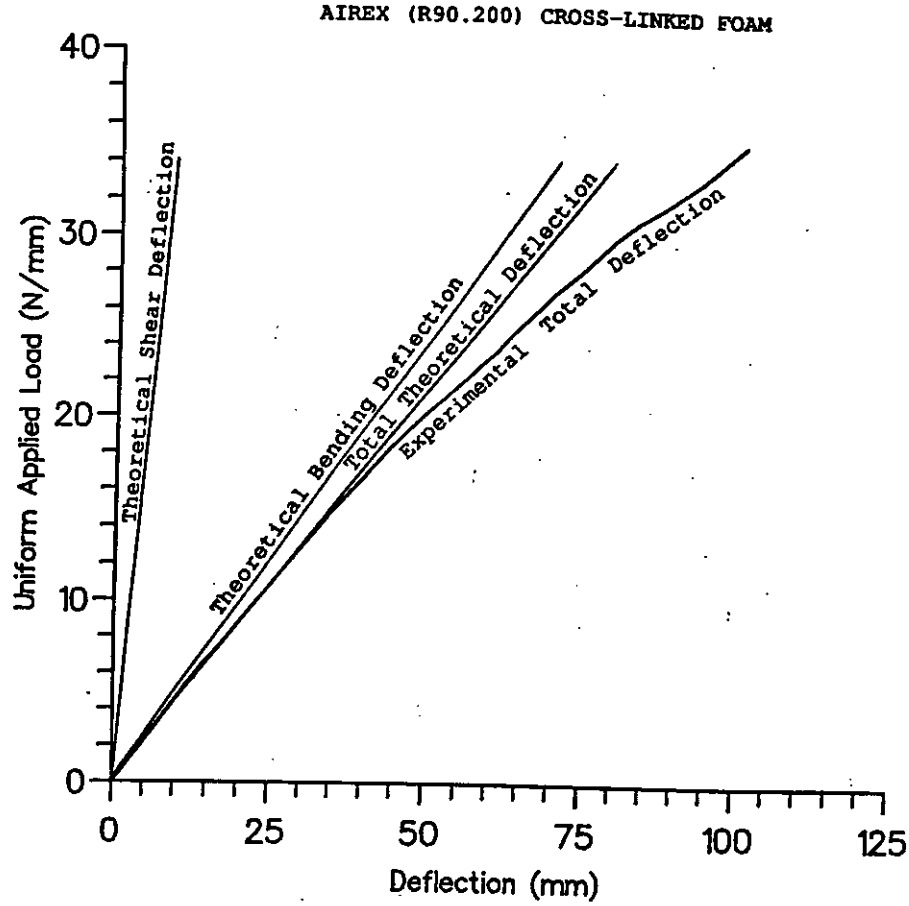

Figure 3.12 Shear Stiffness versus Deflection for RNLI Sandwich Beam

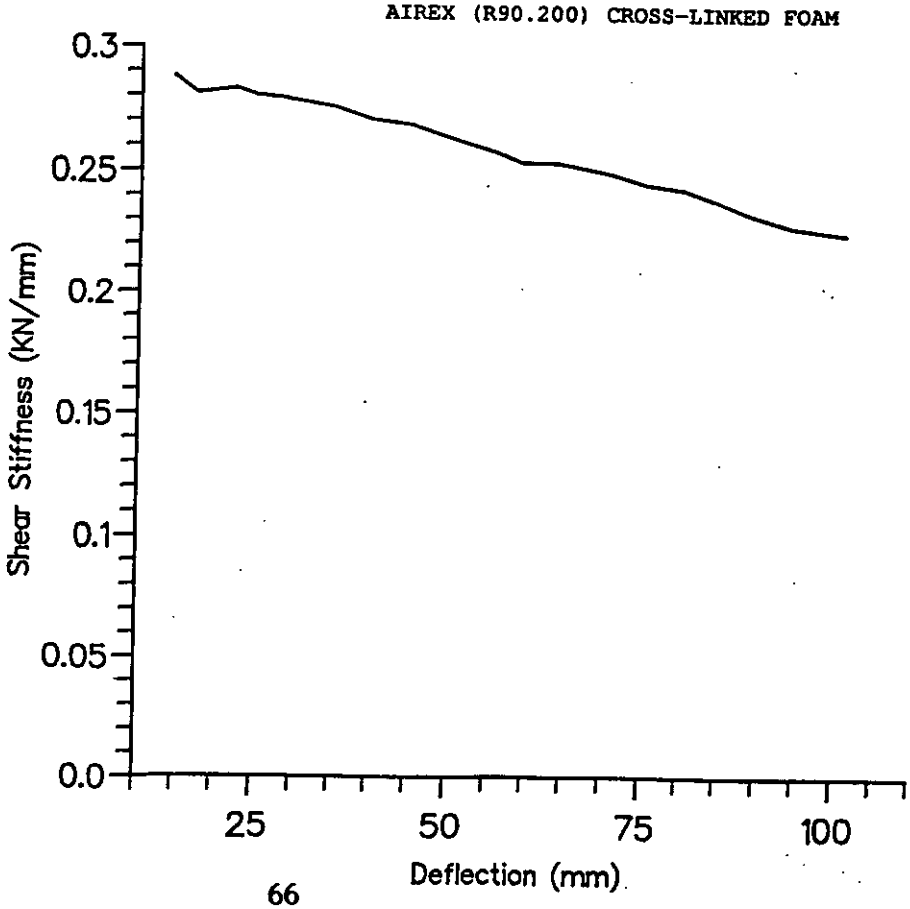

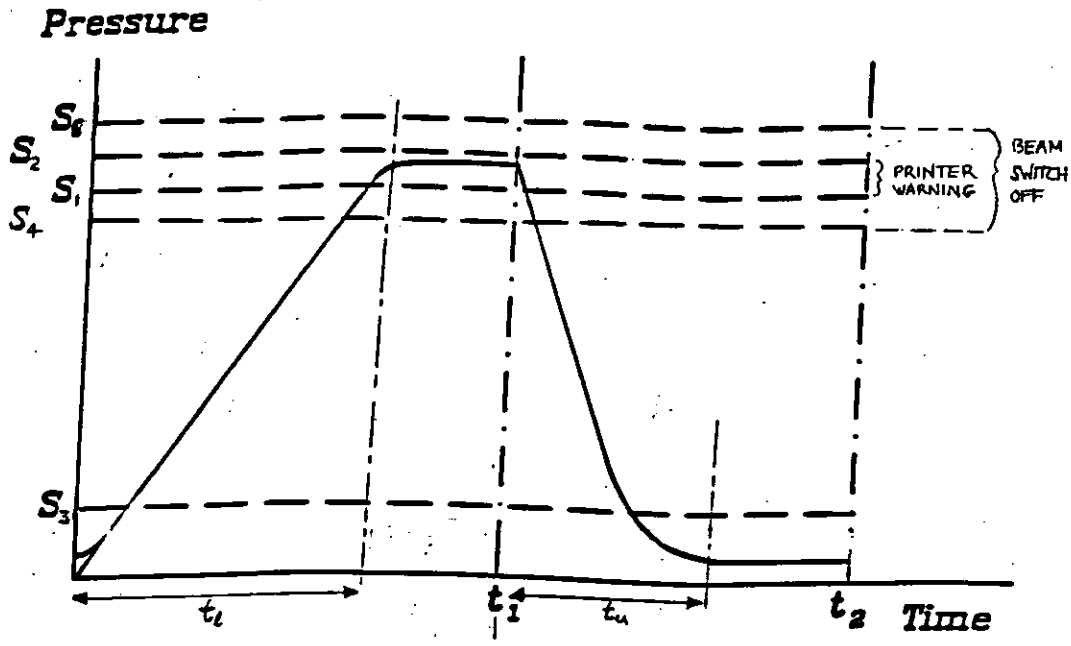

Figure 4.1 : The variation of pressure with time in a complete cycle.

Figure 4.2 Typical Deflection versus Number of Cycles curve

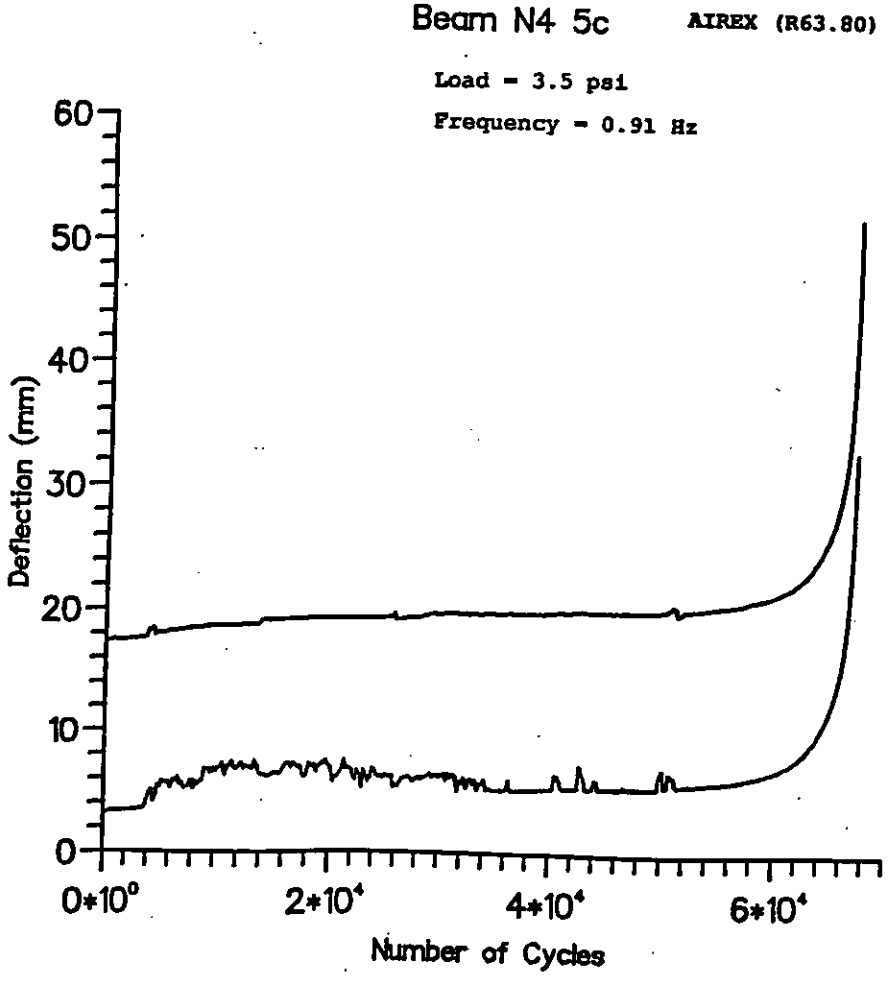

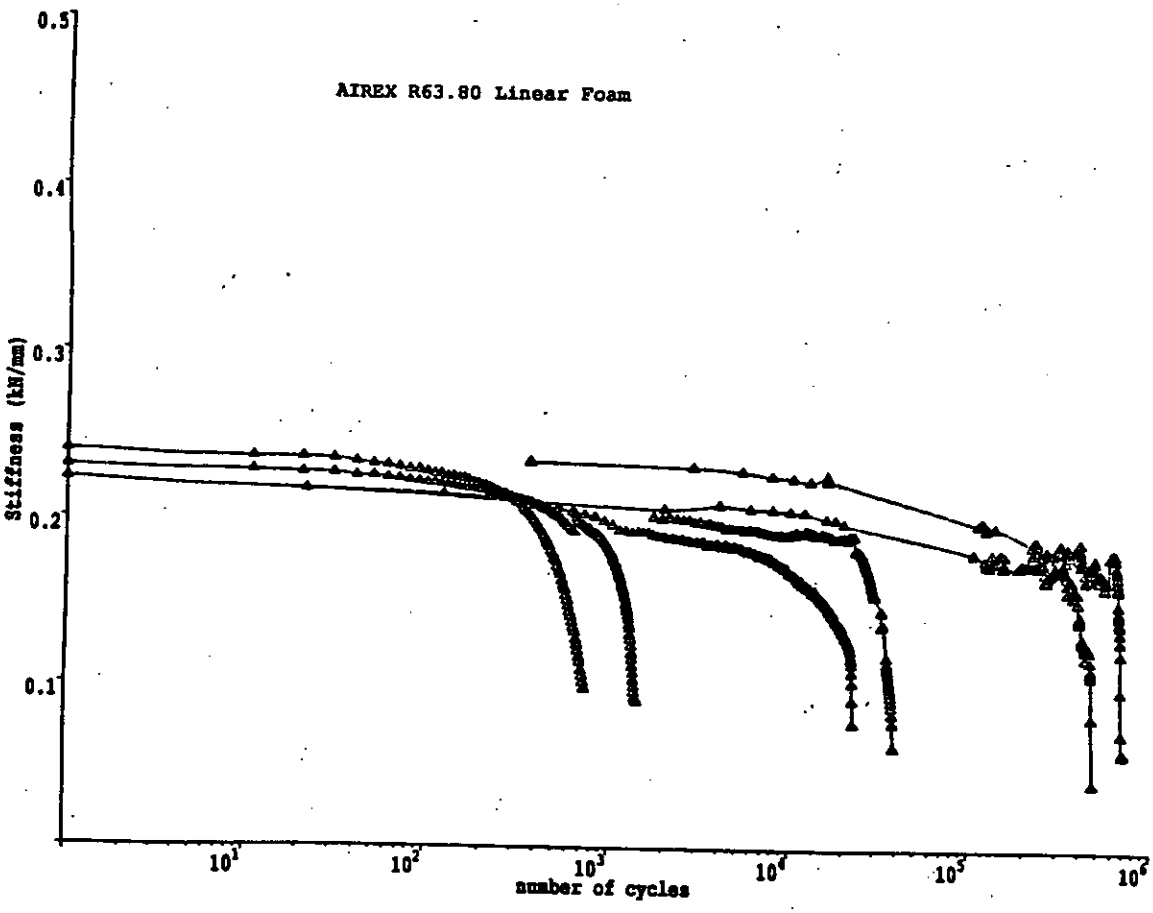

Figure 4.3 The variation of stiffness with cycle number for a selection of beams fatigue tested under different loadings.

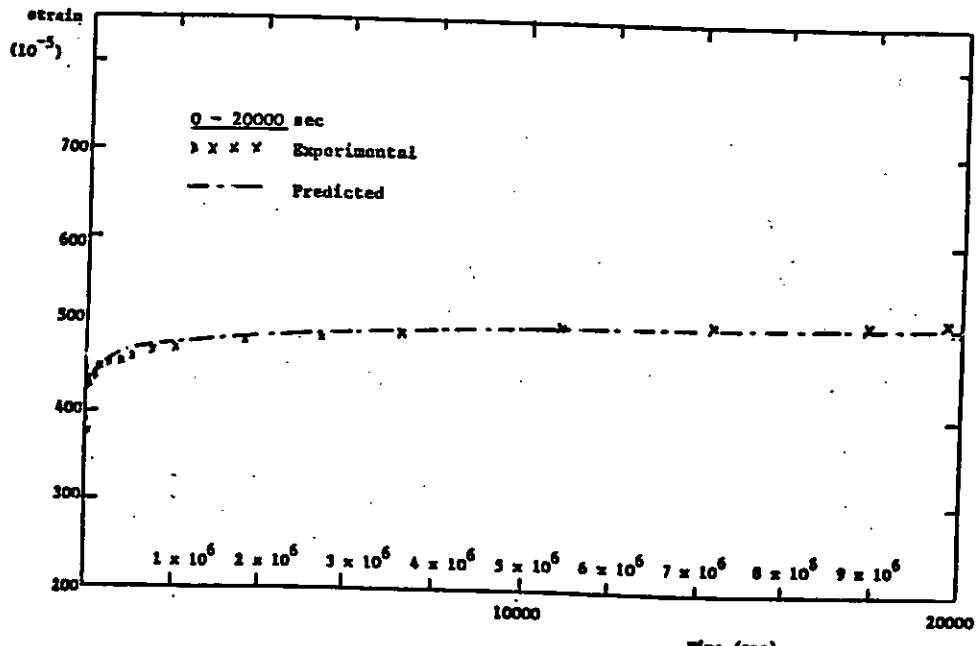

Figure 4.4 Creep of two-directionally reinforced laminates. (Specimen 2 x 28 along, 56 across, 2. Longitudinal glass volume fraction 0.0507 Transverse glass volume fraction 0.0496 Tensile stress 4420 lb/in^2)

Figure 4.5 Typical Beam Distortion
Airex R63.80 Foam Core

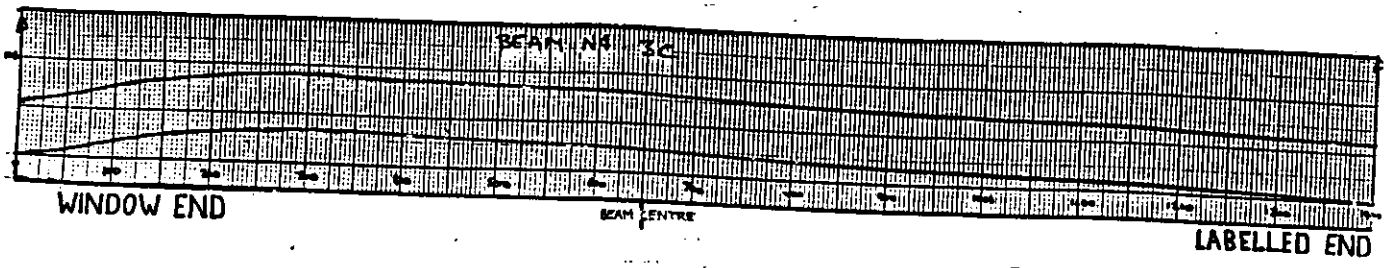

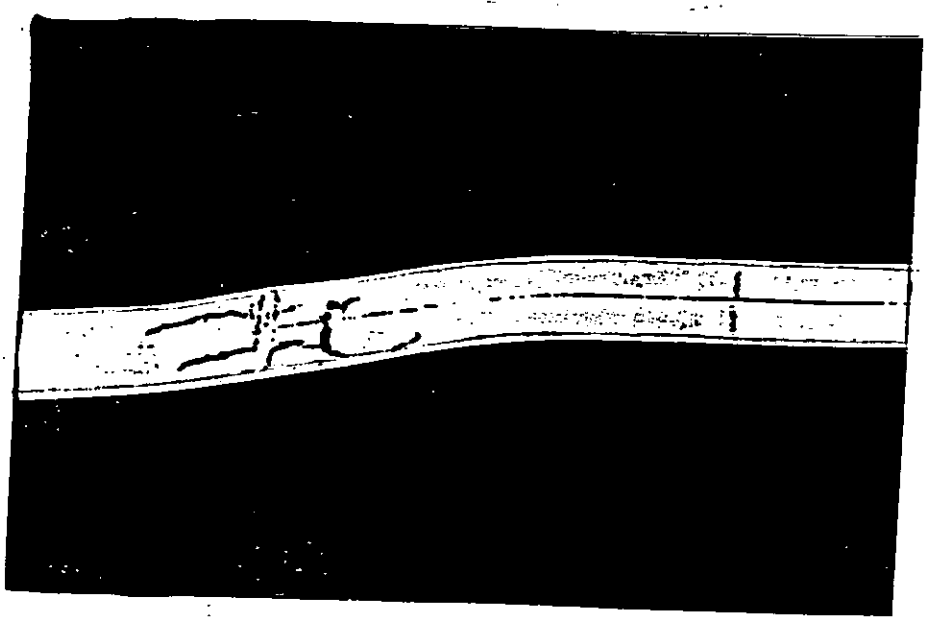

a)

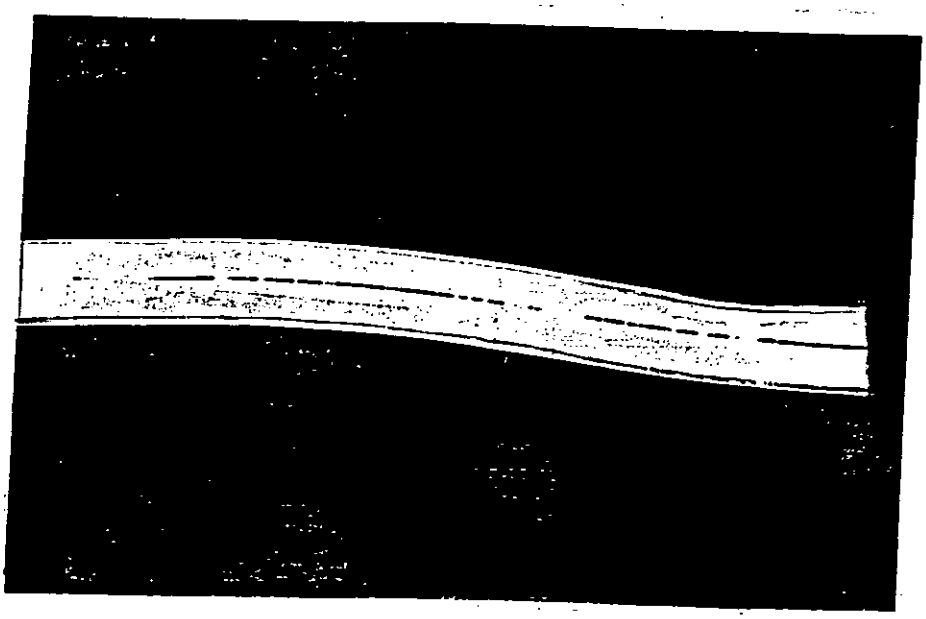

b)

Figure 4.6 : Examples of different failure types of fatigue tested beams.
(a) an obvious cracking, (b) plastic deformation.
AIREX R63.80 Foam Core

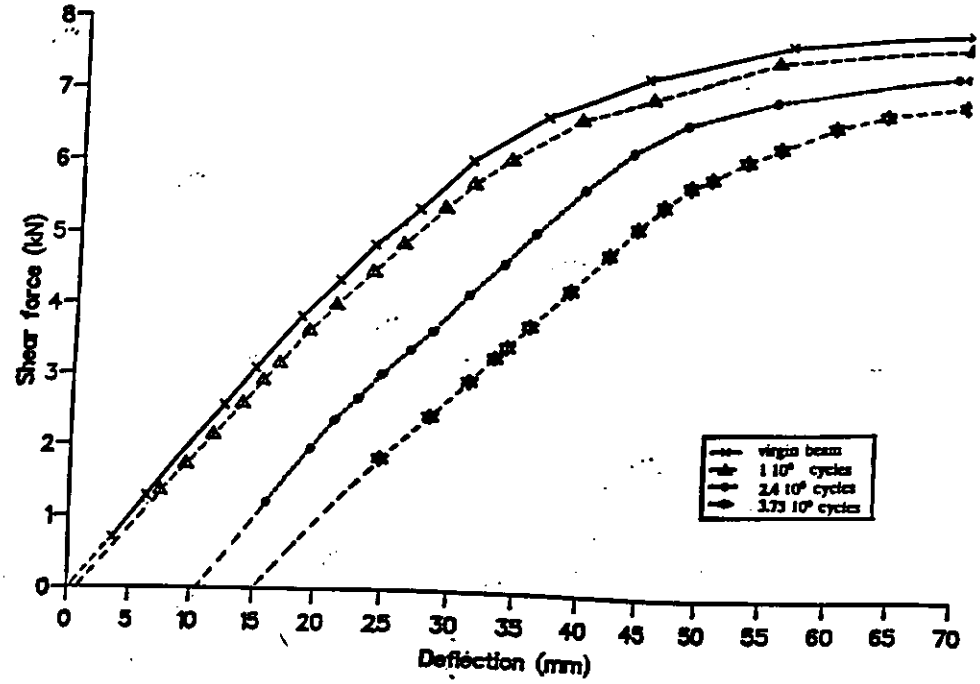

Figure 4.7 : Shear force versus deflection curves obtained from the static test for the three pre-fatigued specimens and a virgin beam.

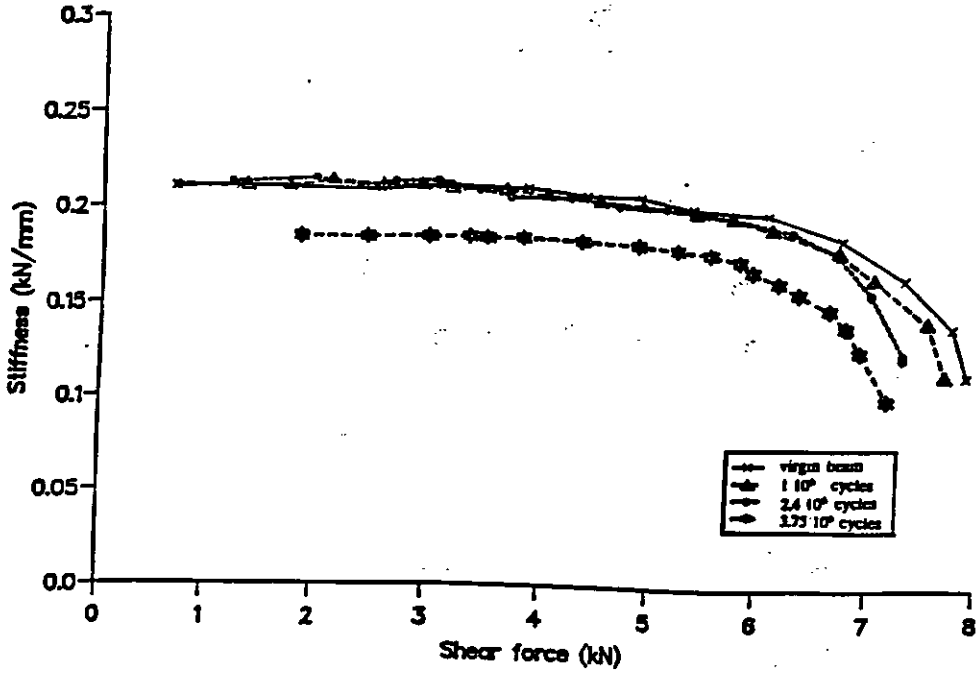

Figure 4.8 : The variation of stiffness with shear force obtained from the static test for the three pre-fatigued specimens and a virgin beam.

Figure 4.9 : S-N curves for Airex R63.80 Foam Core

a) MEAN LOAD versus NUMBER OF CYCLES for RNLI Sandwich Beam

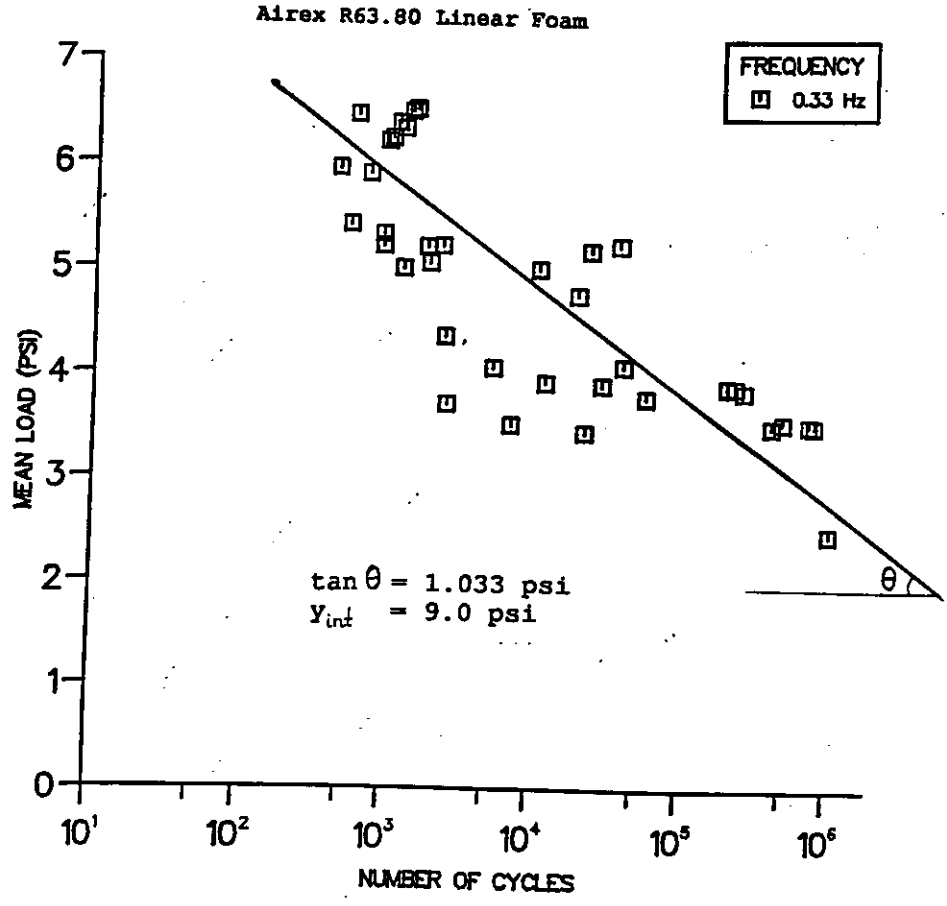

b) MEAN LOAD versus NUMBER OF CYCLES for RNLI Sandwich Beam

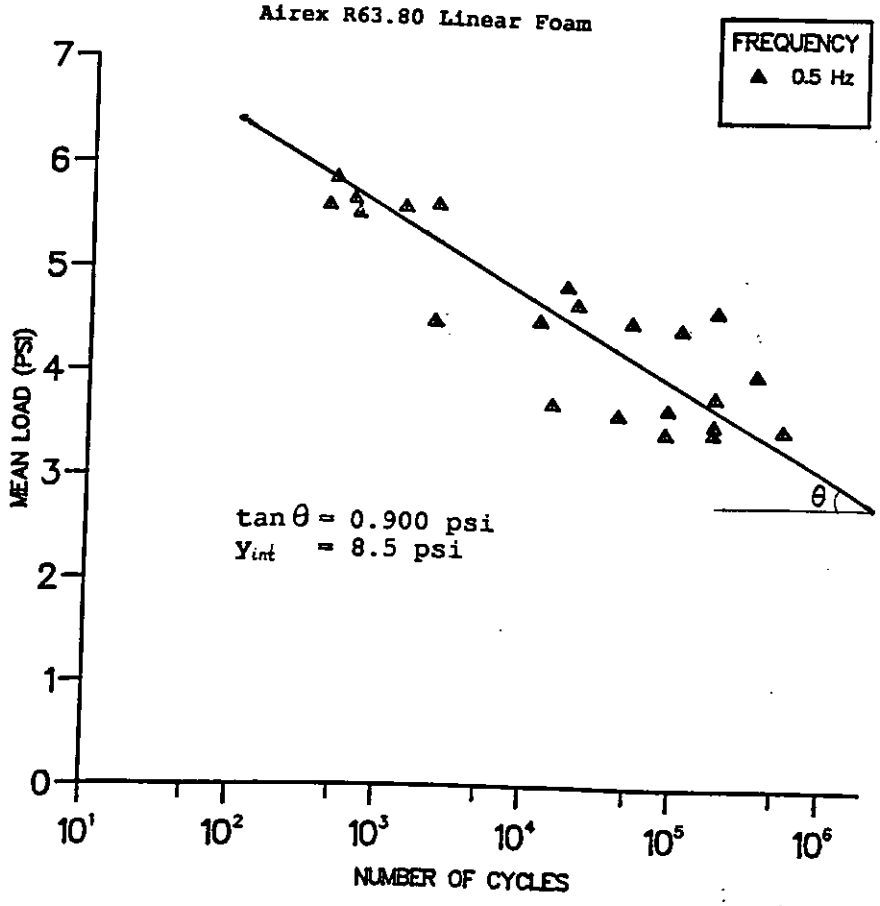

c) MEAN LOAD versus NUMBER OF CYCLES for RNLI Sandwich Beam

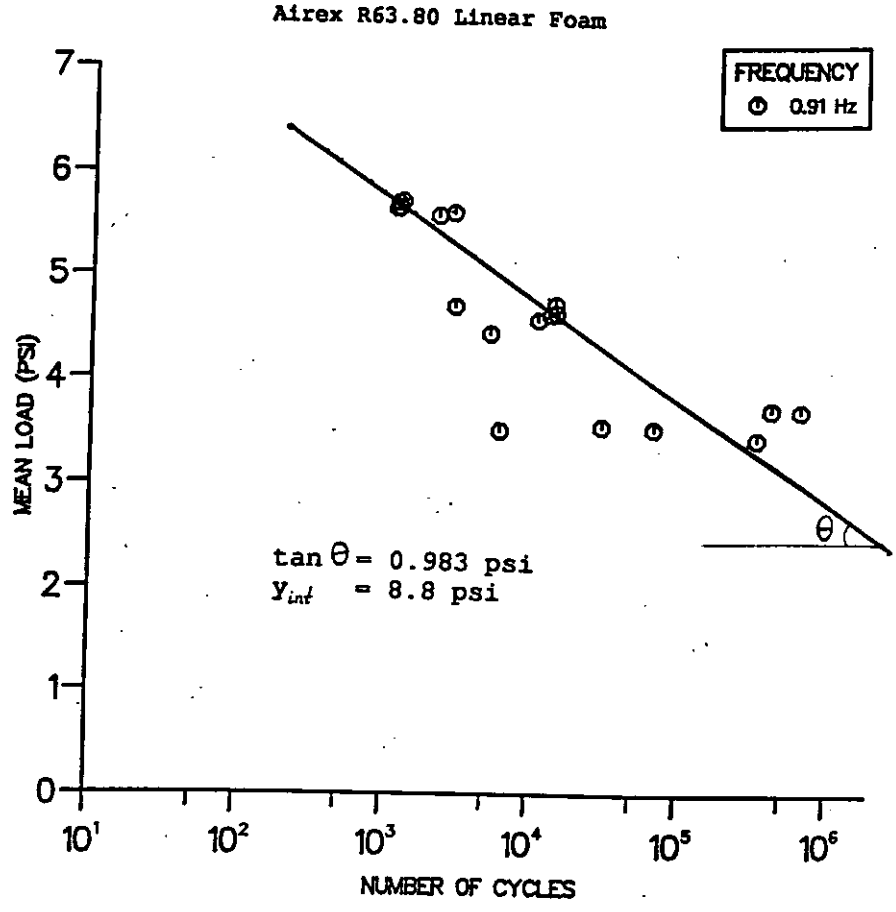

Figure 4.10 NORMALIZED LOAD versus NO. of CYCLES

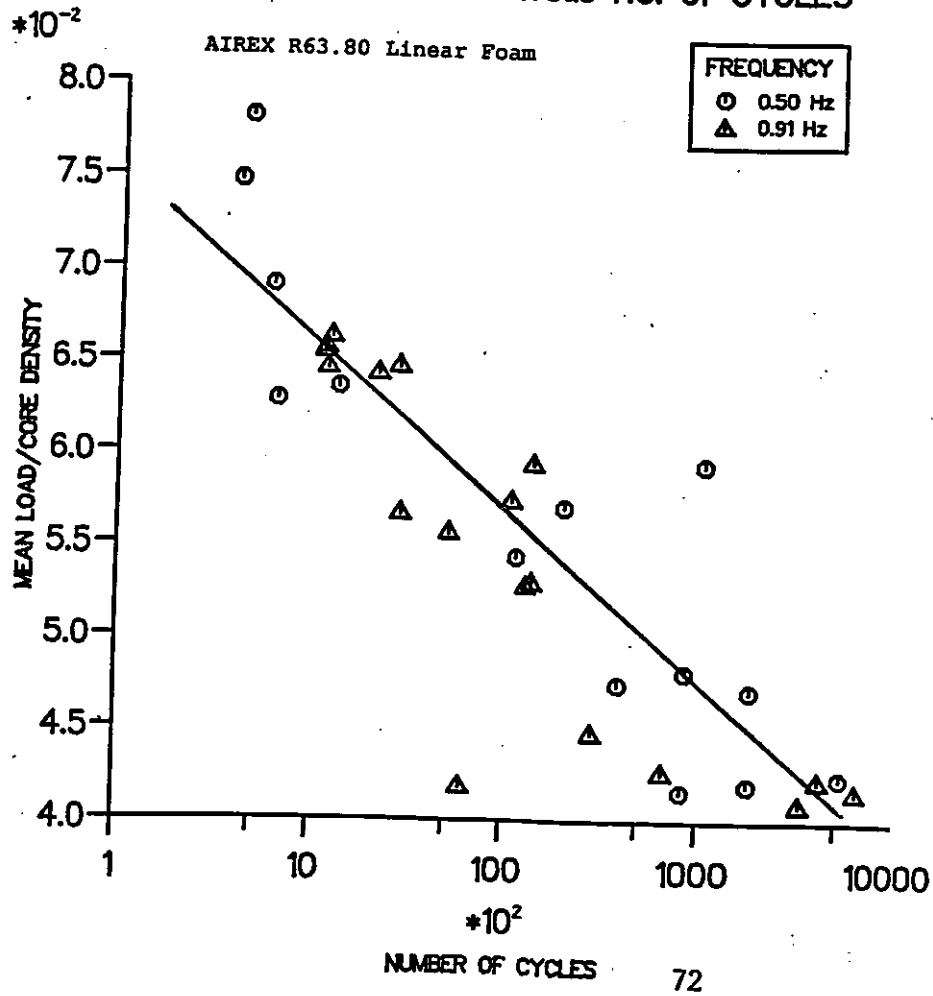

Figure 4.11 TYPICAL VARIATION IN APPLIED LOAD DURING CYCLING

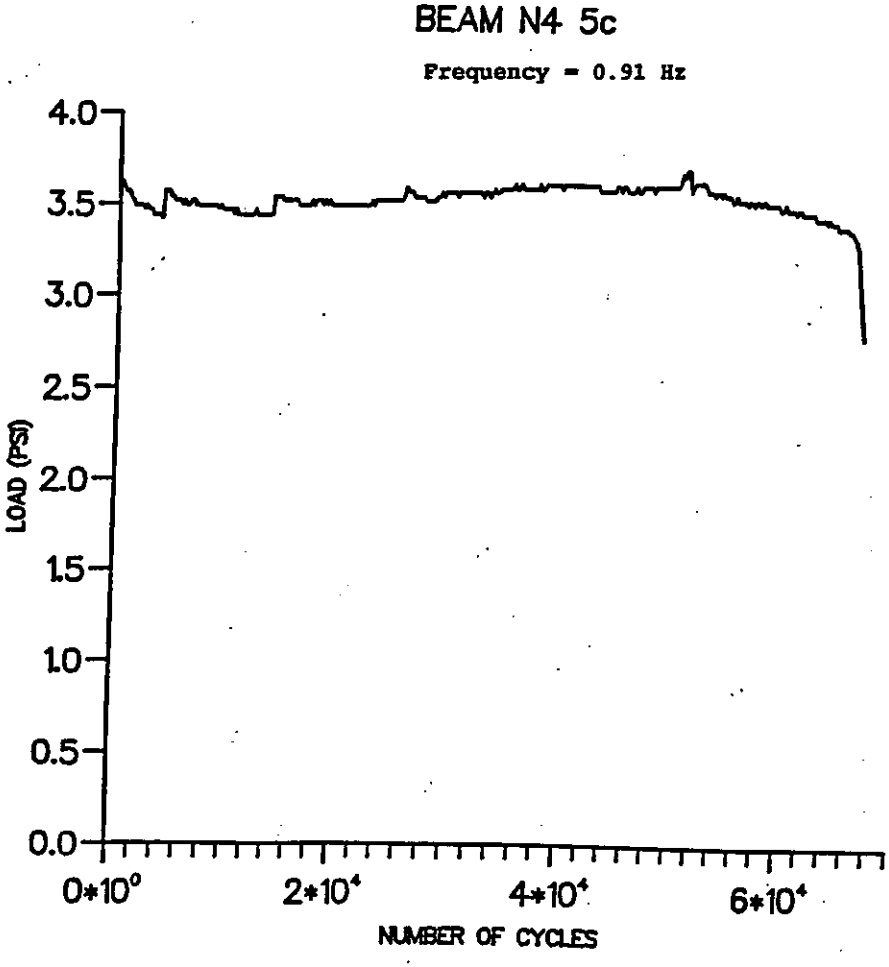

Figure 4.12 : Effect of Frequency on Fatigue Lifetime

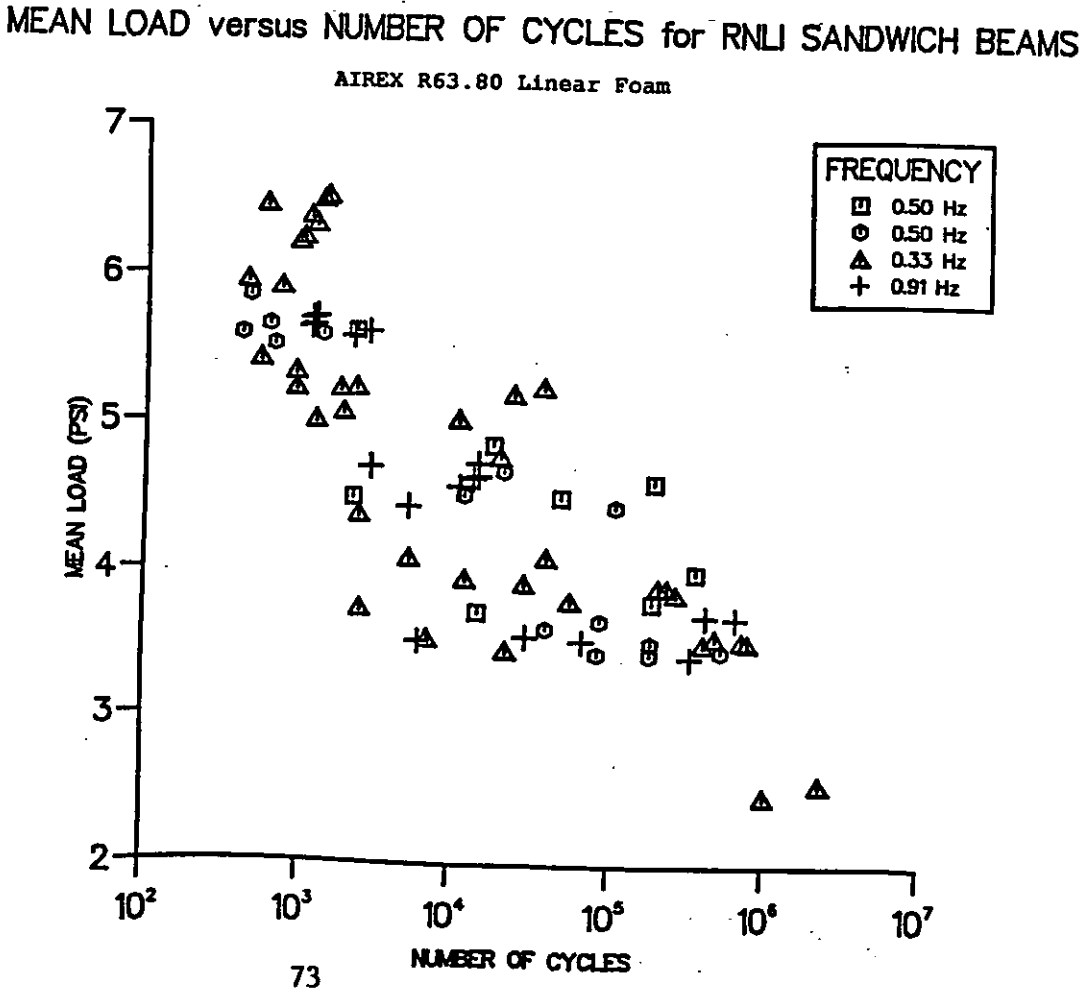

Figure 4.13 Typical Deflection versus Number of Cycles curve

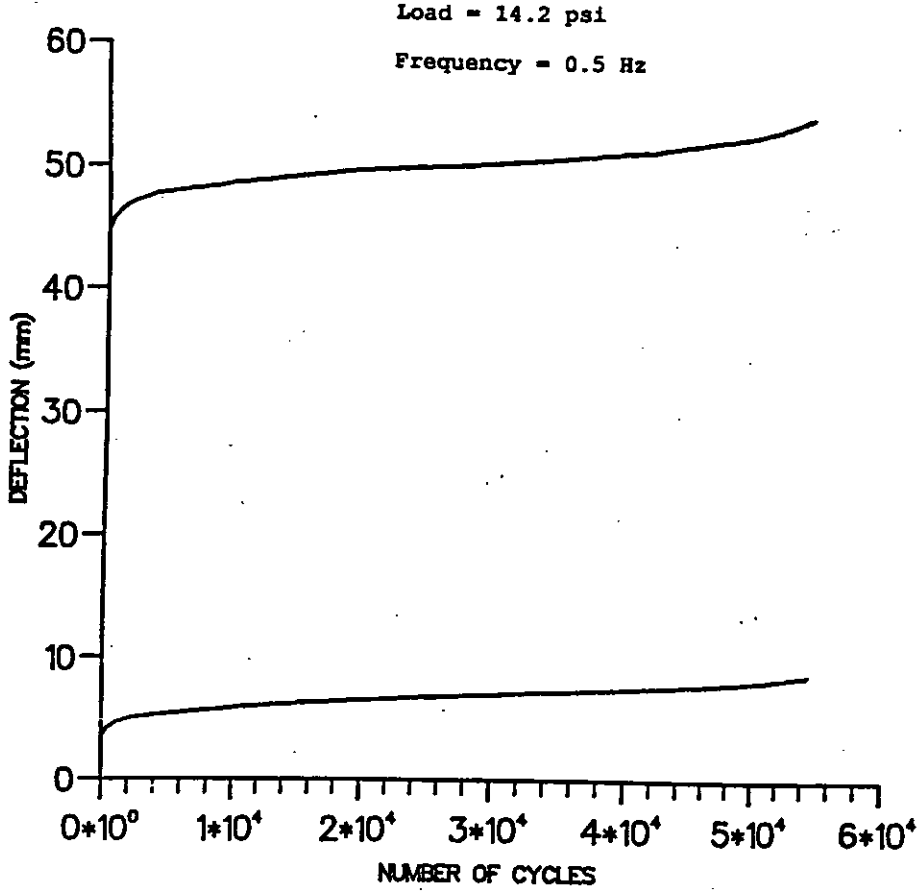

Figure 4.14 STIFFNESS versus No. of CYCLES : Airex R90.200 Core
Frequency = 0.50 Hz

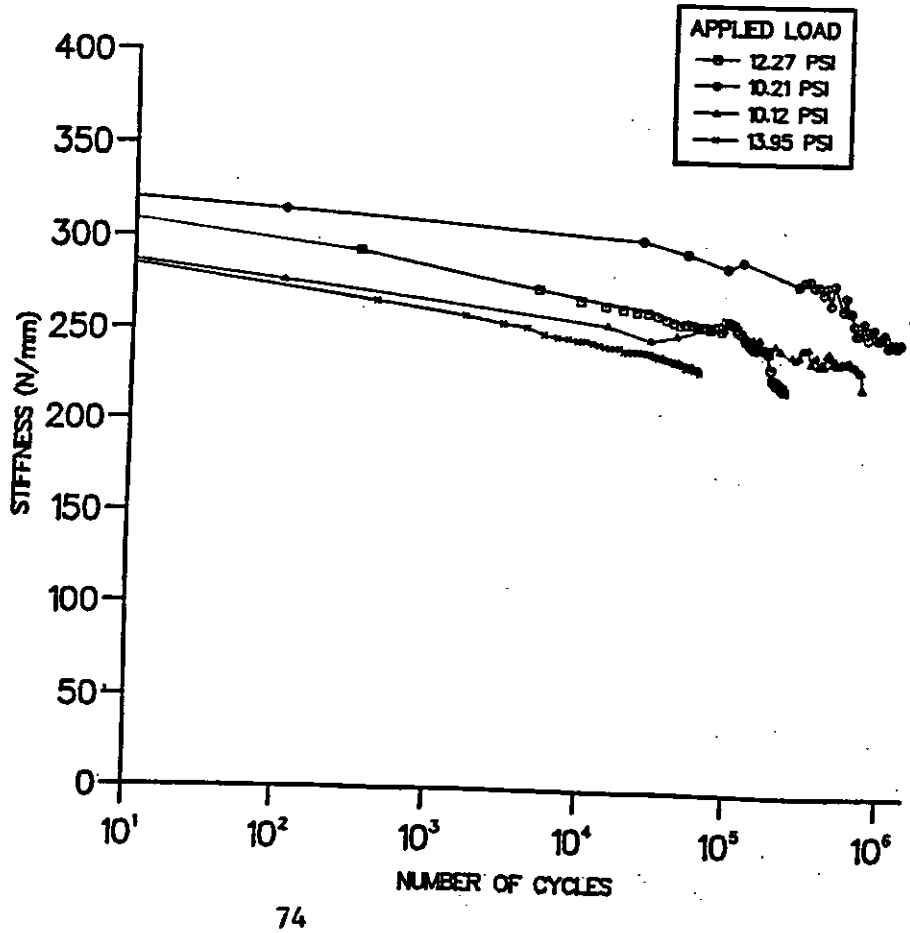

Figure 4.15 MEAN LOAD versus NO. of CYCLES

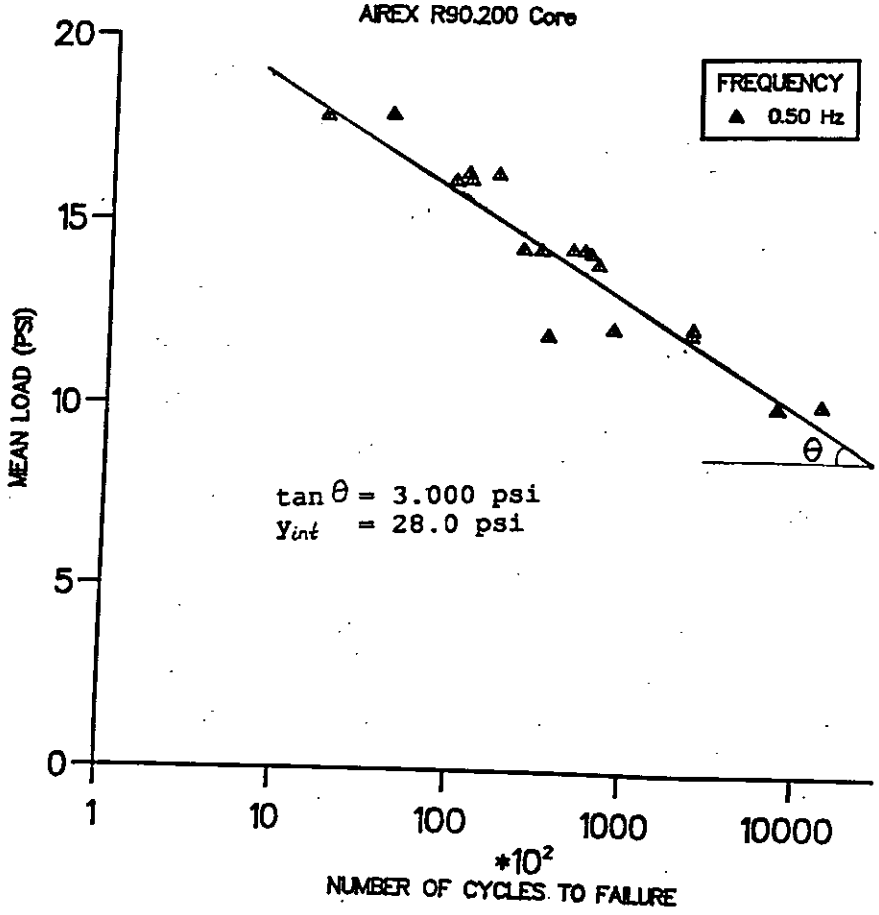

Figure 4.16 : DNV Fatigue Data

(Source : Reference 40)

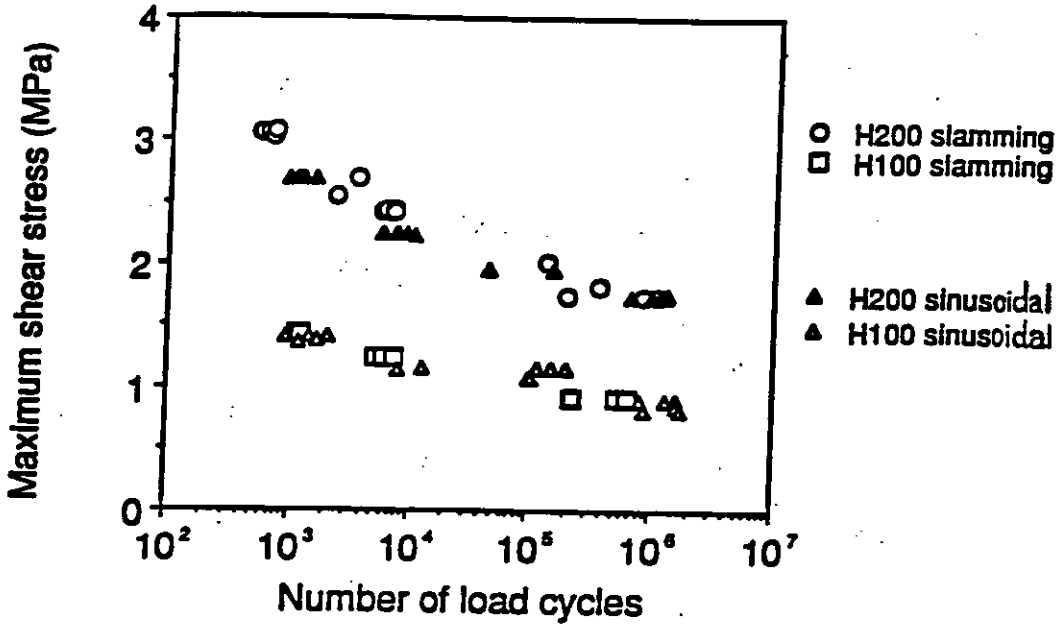

a) Slamming fatigue and sinusoidal fatigue lifetime data

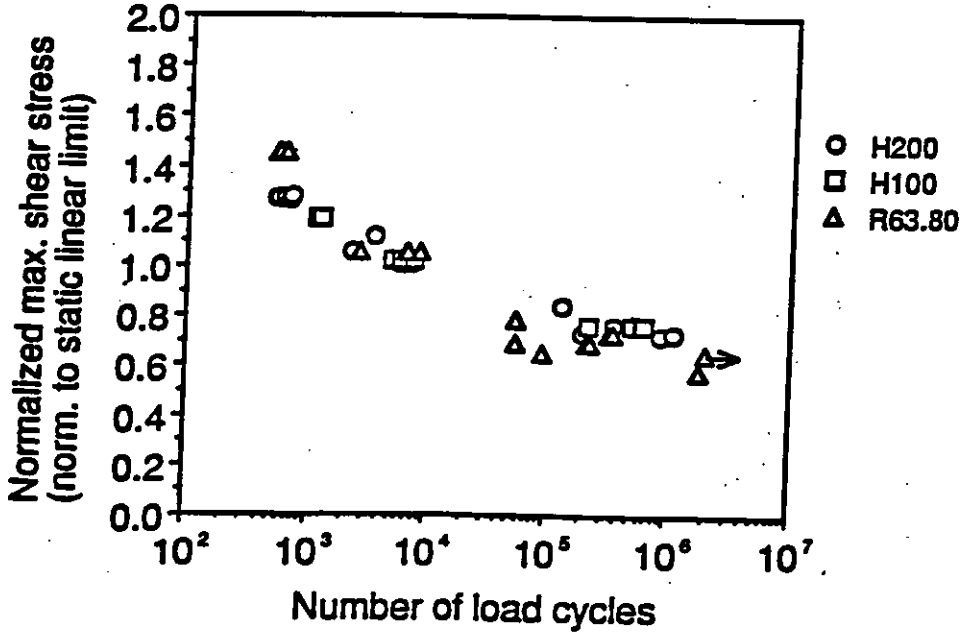

b) Normalized slamming fatigue lifetime data

Figure 4.17 : Fatigue Data

a) SHEAR STRESS versus No. of CYCLES

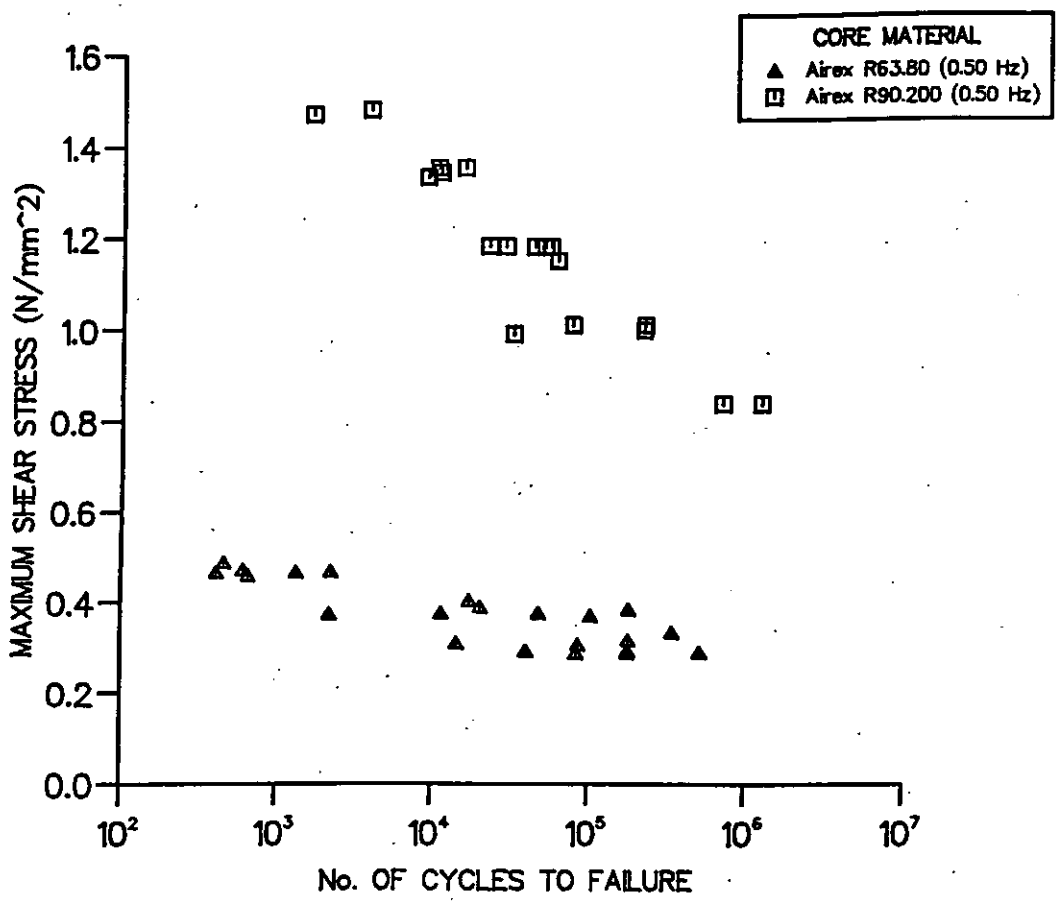

b) NORMALISED SHEAR STRESS versus No. of CYCLES

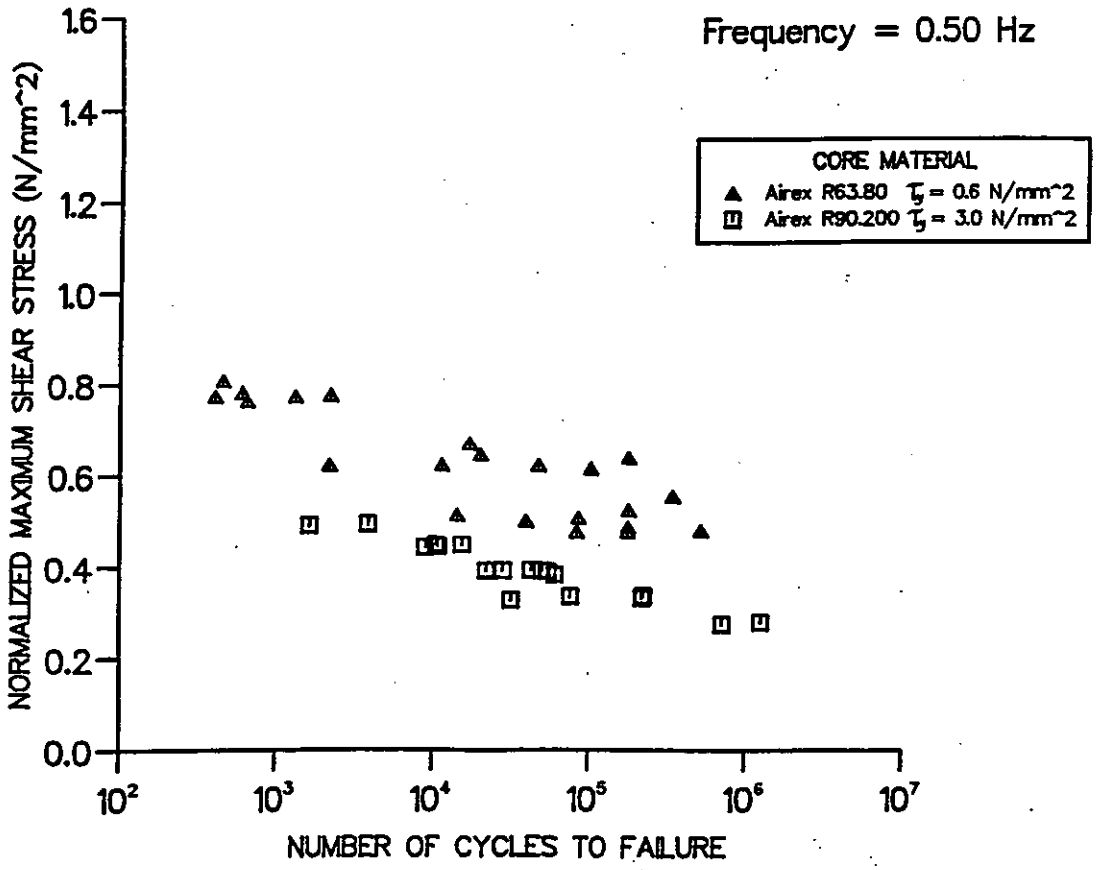

APPENDIX

DESCRIPTION OF THE APPARATUS

The testing machine in its final form is illustrated diagrammatically in Fig. 1. A substantial steel framework (a) supports the test beam via rocking bearings (b). Equal loads are applied at eight points by means of rams (c) driven by compressed air. At the point where each load or reaction is applied to the beam there is a flat rubber-faced plate (d), 200 mm x 50 mm, which is free to rotate. These plates are intended to accommodate changes in the slope of the surface of the beam and to distribute the load sufficiently to avoid problems of indentation.

Deflections are monitored by a transducer mounted on a swivelling arm attached to the mid-point of the beam.

There are three identical test rigs, which can operate simultaneously.

The air supply system is shown diagrammatically in Fig. 2. The diameter of each ram cylinder is 125 mm and the maximum air pressure is 80 psi or 0.552 N/mm^2. With eight rams acting on a surface area of 1300 x 200 mm this corresponds to 30.2 psi or 0.208 N/mm^2 on the surface of the beam.

The air supply is controlled manually by the shut-off valve and the two adjusting valves, one of which sets the maximum pressure on the 'loading' side of each ram, while the other controls the constant back-pressure on the 'unloading' side. A solenoid also controls the main pressure line to the rams. It has two positions; one allows compressed air to reach the rams; the other shuts off the supply of air and releases the air from the rams, down to a preset residual pressure. A PC is used to operate this solenoid as required in order to maintain the magnitude and frequency of the loading cycle.

The control system is based on the notional pressure-time graph shown in Fig. 3. This represents a single load cycle ideally occupying about 1 second. The solenoid allows the main pressure to rise for an interval t_1; the air pressure is then released for an interval t_2 and the cycle is then repeated. Thus control is maintained primarily by adjusting the time intervals t_1 and t_2, and the maximum attainable value of the air pressure. In addition there are several automatic checks. For example:

If the maximum pressure lies outside the bounds S_3 and S_4 a warning is given.

If the maximum pressure lies outside the bounds S_2 and S_5 an alarm is sounded and the experiment is stopped.

If the minimum pressure is above S_1 a warning is given.

If the deflection exceeds a preset limit the experiment is stopped.

As a check on the effectiveness of the loading system, two of the rams on each beam apply load through load cells. One is placed nearest the midspan, the other nearest one end of the beam. The output from these cells, like that from the displacement transducer, is monitored by the PC.

The controlling computer program was written in-house. In addition to controlling the air supply and monitoring the loads and deflections, it provides a variety of modes of recording the progress of the experiment. For example, the pressure-time graph for a single cycle can be examined, or the results (loads, pressures and deflections) for a selected set of cycles can be recalled for detailed examination. All of the records are stored for evaluation at the end of the test run. The outputs from each of the three simultaneous test runs can be examined and controlled independently.

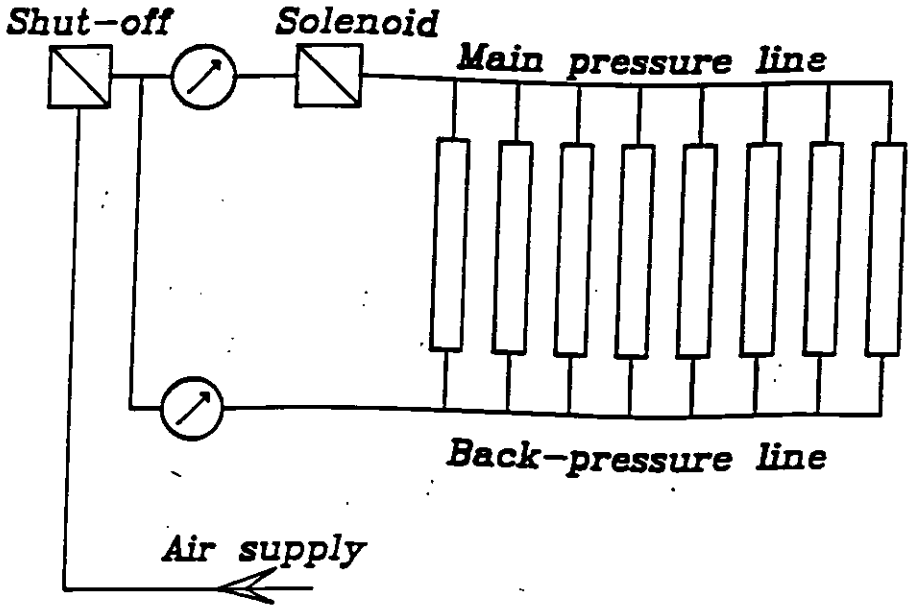

Air supply system

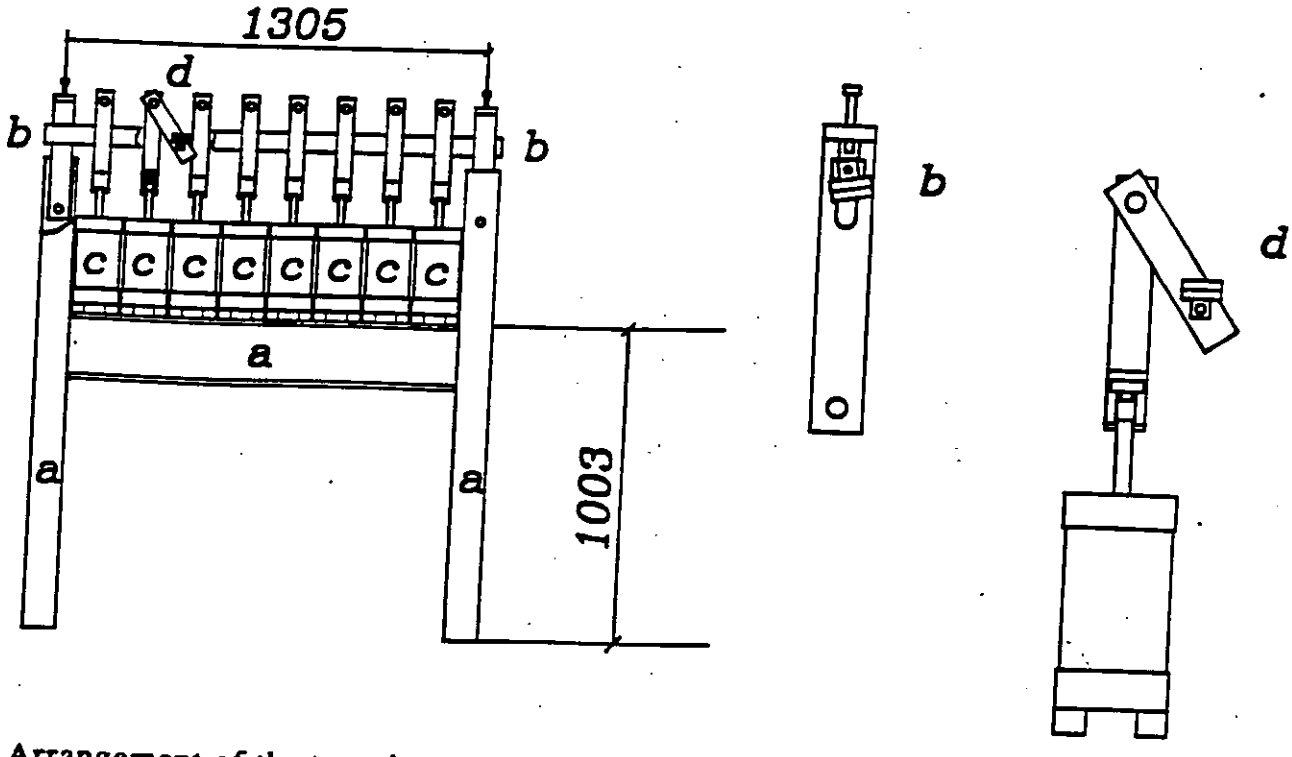

Arrangement of the test rig